NACA

RESEARCH MEMORANDUM

HIGH-SPEED CASCADE TESTS OF A BLADE SECTION DESIGNED FOR TYPICAL HUB CONDITIONS OF HIGH-FLOW TRANSONIC ROTORS

By Melvyn Savage, A. Richard Felix, and James C. Emery

Langley Aeronautical Laboratory
Langley Field, Va.

NATIONAL ADVISORY COMMITTEE
FOR AERONAUTICS

WASHINGTON

September 28, 1955

NACA RM L55F07

NATIONAL ADVISORY COMMITTEE FOR AERONAUTICS

RESEARCH MEMORANDUM

HIGH-SPEED CASCADE TESTS OF A BLADE SECTION DESIGNED FOR TYPICAL HUB CONDITIONS OF HIGH-FLOW TRANSONIC ROTORS

By Melvyn Savage, A. Richard Felix, and James C. Emery

SUMMARY

High-speed cascade tests were made of a blade section designed specifically for conditions typical of the hub section of high-flow transonic rotors. This blade section has a camber of 1.8, a maximum thickness of 8 percent, an A_6I_{4b} mean line, and a thickness distribution which has its maximum thickness at the 65-percent-chord point and is somewhat similar to the NACA 65-series thickness distribution reversed. Since an appraisal of the relative merits of the A_{10} (constant loading chordwise) and the A_6I_{4b} mean lines indicated no obvious advantage of one over the other for transonic hub conditions, the selection of the A_6I_{4b} mean line was quite arbitrary. The testing of either mean-line type will provide information on the effects of local surface Mach numbers on blade performance.

The tests were made at four combinations of inlet angle and angle of attack at a solidity of 1.5. The inlet angles ranged from 26.9° to 34.1°. Measurements of surface pressure distribution, profile momentum loss, and turning angle, as well as schlieren photographs, were made for inlet Mach numbers ranging from 0.30 to the blade choke condition.

The results of these tests show that turning angles of the order of 40° can be accomplished without severe momentum loss for inlet Mach numbers up to 0.70 at an inlet angle of 26.9° and up to 0.75 at an inlet angle of 30.0°. At inlet angles from 30.0° to 34.1° momentum-loss coefficients of approximately 0.03 were obtained at an inlet Mach number of 0.80. A surface Mach number of approximately 1.26 near the leading edge of the blade appeared to be close to the separation limit for the curvature conditions which existed near the leading edge. The high-speed turning angle for a typical test was effectively estimated from low-speed cascade data. The variation in turning angle with inlet Mach number for momentum-loss coefficients up to approximately 0.03 is small (at most, about ±0.5°).

INTRODUCTION

In high-flow transonic compressors with low hub-tip ratios large aerodynamic differences exist between flow conditions at the hub and tip sections. At the tip the inlet angles and inlet Mach numbers are relatively high, and low solidities and thin, low-camber blade sections are generally used. Hence, the minimum passage area between blades at the tip is almost invariably greater than the inlet-stream-tube area and there is no choking problem. At the hub, inlet angles are low, and lower inlet Mach numbers are encountered. High solidities and relatively thick, high-camber blade sections are used to meet pressure-ratio and stress requirements. This combination of high blade thickness and high solidity results in a blade passage area which can be less than the inlet-stream-tube area. Hence, choking can present a real problem in the hub region.

The purpose of this investigation was to study the flow phenomena associated with conditions typical of a high-flow transonic rotor hub. This study was made by analyzing the results of low-inlet-angle, high-solidity, high-speed cascade tests of compressor blading specifically devised for such hub conditions. The blade section tested had a lift coefficient C_{l_o} of 1.8 and an A_6I_{4b} mean line (some rearward loading). The blade section was 8 percent thick with maximum thickness located at 65 percent chord. This thickness distribution is very similar to a reversed NACA 65-series thickness distribution.

The experimental data were obtained in the 7-inch high-speed cascade tunnel at the Langley Laboratory at a solidity of 1.5 for four combinations of air-inlet angles and angles of attack. The inlet angles ranged from 26.9° to 34.1°. Blade-surface pressure distributions, profile momentum losses, and turning angles were measured and schlieren observations were made at inlet Mach numbers from 0.3 to choking.

SYMBOLS

A	area, sq ft
A_T	minimum area in blade passage, sq ft
C_{w_1}	momentum-loss coefficient
C_{l_o}	camber expressed as isolated-airfoil lift coefficient
c	chord length, ft
F_c	ratio of momentum-loss coefficient to integrated total-pressure-loss coefficient

M	Mach number
P	total pressure, lb/sq ft
p	static pressure, lb/sq ft
q	dynamic pressure, lb/sq ft
R_{LE}	leading-edge radius, percent chord
R_{TE}	trailing-edge radius, percent chord
S	surface pressure coefficient, $\frac{P - p_l}{q_l}$
S_{cr}	surface pressure coefficient corresponding to local sonic velocity
t	maximum blade thickness, ft
T	total temperature, $^{\circ}R$
SWF	specific weight flow, lb/sec/sq ft of frontal area
w	wake width, ft
x	blade-section abscissa, percent chord
y	blade-section ordinate, percent chord
α	angle of attack, deg
β	air inlet angle, deg
θ	turning angle, deg
σ	solidity

Subscripts:

d	design
h	hub
l	local
m	maximum
R	relative to rotor, rotor coordinates

t	tip
w	blade wake
1	upstream station
2	downstream station

DESIGN CONSIDERATIONS FOR HUB BLADE SECTIONS

General Discussion

In the calculation of velocity diagrams for an inlet stage of a multistage compressor of high specific-weight-flow capacity, a judicious choice must be made of (1) rotational speed and (2) hub-tip ratio. An increase in rotational speed results in an increase in hub inlet angle which tends to alleviate hub choking, but tip relative Mach number also increases making the design of the tip increasingly difficult. A decrease in hub-tip ratio reduces the inlet axial velocity and tip Mach number but also tends to reduce the hub inlet angle, thereby increasing the possibility of hub section choking. Other problems which arise include the selection of the average value of total-pressure ratio to be produced and its radial distribution as well as the selection of the optimum combination of camber and solidity, mean-line shape, and blade-section thickness distribution.

Figure 1 shows the variation of rotor-tip relative inlet Mach number with specific weight flow for various hub inlet angles for an inlet hub-tip ratio of 0.35 for high-flow transonic rotors with no inlet guide vanes. It may be seen that high specific weight flow requires a compromise between high inlet Mach number at the tip and low inlet angle at the hub. For tip inlet Mach numbers of the order of 1.2, the hub section must operate at inlet angles of 30° and less. Inlet Mach numbers for the hub sections will range from 0.65 to over 0.80.

Solidities of the order of 1.5 and higher are necessary at the hub to assure a reasonably high tip solidity; otherwise, an increase in tip chord would be necessary which would be undesirable from structural considerations. A moderately thick blade is required to meet strength and vibration requirements.

It is shown in reference 1 that the combination of low inlet angle, high solidity, and moderately thick blade results in contraction ratios less than unity; that is, the minimum flow area in the blade passage is less than the stream-tube area entering the blade passage. For moderate subsonic inlet Mach numbers, contraction ratios much below unity could result in a choked condition. Even if choking does not occur for

contraction ratios less than unity, the average Mach number of the flow in the minimum passage area must be greater than the inlet Mach number. Since blade-surface Mach numbers are primarily determined by passage area and surface curvature, the increase in average Mach number is reflected in increased surface Mach numbers. By manipulation of blade thickness distribution, mean-line shape, inlet angle, solidity, and angle of attack, some control over this situation can be maintained.

Operating Conditions and Camber Selection

The selection of the type of blading for transonic high-flow rotor-hub sections requires specific knowledge of the cascade conditions (inlet angles, solidities, and cambers) typical of the hub region. For the case at hand, typical conditions were selected from a preliminary design calling for a specific weight flow of 37.5 pounds per second per square foot of frontal area, an inlet hub-tip ratio of 0.35, and a tip relative inlet Mach number of 1.1. In this design the hub conditions were approximately as follows: inlet angle 30°, solidity 1.5, turning angle 40°, and inlet Mach number 0.75. These conditions are somewhat similar to those of the high-flow transonic rotor of reference 2.

The amount of camber required for an inlet angle of 30°, a solidity of 1.5, and a turning angle of 40° was investigated using the low-speed cascade data of references 1 and 3. These data show that a design lift coefficient of 1.8 produces turning angles of 37.6° and 40.0° at design angle of attack for blade sections having A_{10} and A_2I_{8b} mean lines, respectively. (See ref. 4 for mean-line notation system.) Hence, a C_{l_o} of 1.8 was selected as being representative of typical hub cambers.

Thickness Distribution

Since flow separation in compressor cascades results when the boundary layer is unable to negotiate the pressure-rise conditions which occur chordwise along the blades, it is desirable to keep this pressure rise and, hence, surface Mach number to a minimum. Therefore, a main objective in the selection of a thickness distribution was to keep surface Mach numbers low by maintaining low surface curvature over the forward portion of the blade. To accomplish this end a thickness distribution was derived which was considerably thinner in the forward portion of the blade than the types of thickness distribution commonly used for subsonic blading.

Figure 2 shows a comparison of the derived thickness distribution used in this investigation (hereinafter referred to as the T1 thickness distribution), the conventional subsonic NACA 65-series thickness distribution (ref. 5), and the thickness distribution of an inboard section of the transonic rotor of reference 6 (section DD of ref. 7). All are

scaled up to 10-percent maximum thickness. The T1 distribution is somewhat flatter over the forward 60 percent of the blade chord than that of the DD section of reference 7 and represents a considerable change from the NACA 65-series thickness distribution. It should be noted that the point of maximum thickness for the T1 distribution is rearward at approximately the 65-percent blade-chord station. The T1 distribution is somewhat similar to the NACA 65-series thickness distribution reversed.

The coordinates for the T1 thickness distribution are presented in table I for the 8-percent-thick section. Direct scaling may be used for other thicknesses. The suggested variation of leading- and trailing-edge radii with maximum thickness is shown in figure 3. This thickness distribution was used in the high-flow transonic rotor of reference 2.

Mean-Line Shape

The influence of contraction ratios of less than 1.00 on surface Mach numbers is clearly indicated in the extrapolated pressure distributions for bladings having different mean lines in reference 1. It was shown that high surface Mach numbers do occur near the minimum passage area. Hence, in the selection of a mean line to be used with the T1 thickness distribution, it was necessary to examine the blade passage areas.

For low-inlet-angle high-solidity conditions, the A_6I_{4b} or A_{10} mean line was shown in reference 1 to have greater contraction ratios than the A_2I_{8b} mean line. For example, at $\beta = 30^\circ$, $\sigma = 1.5$, and α_d, A_T/A_1 for the 65-$(12A_2I_{8b})$10 blade was 0.897 compared with 0.918 for the 65-$(12A_6I_{4b})$10 blade and 0.930 for the 65-$(12A_{10})$10 blade. Since this comparison was made for blades having a $C_{l_o} = 1.2$ and using the NACA 65-series thickness distribution, a similar comparison has been made for blades having a $C_{l_o} = 1.8$ and the T1 thickness distribution.

There is a design turning-angle variation of 2.4° between a 1.8 cambered blade with an A_{10} mean line and one with an A_2I_{8b} mean line. To make the turning angles equal would require an increase in C_{l_o} of 0.14 for the A_{10} mean line. Although any comparison of mean-line shapes should be based on the same turning angle, it has been shown in reference 1 that, at low-inlet-angle conditions, the effect of a camber variation of 0.14 on contraction ratio is very slight. Hence, the blade-section comparisons were all made for a camber of 1.8.

Two-dimensional cascade passages were drawn for blades utilizing the T1 thickness distribution in conjunction with the A_{10}, A_6I_{4b}, and A_2I_{8b} mean lines at $\beta = 26.9^\circ$, $\sigma = 1.5$, and design angle of attack, as obtained from low-speed cascade tests, as well as for 2.5° above design angle of attack. The passage areas were measured along an approximation of the stream equipotential lines in the same manner as described in reference 4. These two-dimensional cascade passages are presented in figure 4 with the dashed portion of the figure representing the condition 2.5° above design angle of attack. The location of the minimum passage area and the A_T/A_1 values are indicated. At design angle of attack the value of A_T/A_1 for the A_2I_{8b} blade was 0.948 compared with 0.976 for both A_6I_{4b} and the A_{10} blades. At $\alpha_d + 2.5^\circ$, the A_2I_{8b} blade had a value of A_T/A_1 of 0.964 compared with approximately 0.988 for the other two blades. Hence, from choke-flow considerations, regardless of whether the NACA 65-series or the T1 thickness distribution is used, both the A_6I_{4b} and the A_{10} mean lines should be more desirable than the A_2I_{8b} mean line for the conditions of low inlet angle, high solidity, and the moderate thicknesses required for transonic rotor-hub sections.

The variation in the ratio of A_l/A_1 through the blade passages for the blades having the A_6I_{4b} and the A_{10} mean lines was determined for both α_d and $\alpha_d + 2.5^\circ$ and is presented in figure 5. At design angle of attack (fig. 5(a)) the A_6I_{4b} blade has an extensive region of minimum-area ratio. Hence, on a passage-area basis alone, the A_{10} appears to be a more desirable mean line for high-flow, transonic rotor-hub conditions.

Unpublished high-speed cascade results indicated that, for blades which have contraction ratios less than 1.00, as the inlet Mach number increases the minimum-loss point shifts to higher incidence angles or higher angles of attack than the low-speed design angles (those obtained from an inspection of low-speed cascade pressure distributions to determine the angle of attack where there were no velocity peaks on either surface, ref. 3). Hence, the comparison between area ratios at $\alpha = \alpha_d + 2.5^\circ$ was considered to be more important than that at α_d in the selection of the mean line for testing. At $\alpha_d + 2.5^\circ$ (fig. 5(b)) the A_6I_{4b} blade has a gradually decreasing passage area from the inlet to the minimum-passage-area location, whereas the A_{10} exhibits two minimums of approximately the same value. On the basis of passage area alone at $\alpha_d + 2.5^\circ$, it is difficult to determine which of these two blades would be more nearly optimum.

Blade performance is determined by blade-surface velocities which are affected by both surface curvature and the passage-area effects. The limits of surface curvature and the resulting local blade-surface

Mach numbers that may be tolerated with reasonable efficiency for the particular boundary-layer thickness which exists ahead of the region under consideration have not been established. The A_6I_{4b} blade will have higher curvature in the rearward portion where its minimum passage area occurs. This condition is, of course, undesirable. However, the A_{10} blade will have the undesirable condition of higher curvature in the forward portion, where one of its minimum passage areas occurs, as well as a reoccurrence of a second minimum passage area at the rear of the blade. Which of these conditions is worse is not obvious without test results. Therefore, the selection of which of the two blades to test was rather arbitrary, with either selection capable of providing information on the effects of local surface Mach number on blade performance. The mean-line type chosen for testing was the A_6I_{4b} mean line.

TEST APPARATUS, FLOW MEASUREMENTS, AND TEST PROCEDURE

A schematic diagram of the 7-inch high-speed cascade tunnel at the Langley Laboratory is presented in figure 6. The tunnel span is 7 inches, and for these tests 6 blades were used. Slot suction was provided upstream of the cascade on both floors and side walls. All blade-performance data were obtained using porous side walls with the exception of the schlieren photographs which required the use of glass side walls. The blade section tested was the T1-(18A_6I_{4b})08 blade having a chord length of 4.2 inches. One of the center blades had 22 orifices located at midspan, from which pressure distributions were obtained.

The conditions tested were as follows:

(1) $\beta = 26.9^\circ$, $\alpha = 21.5^\circ$

(2) $\beta = 30.0^\circ$, $\alpha = 24.6^\circ$

(3) $\beta = 34.1^\circ$, $\alpha = 25.0^\circ$

(4) $\beta = 34.1^\circ$, $\alpha = 26.5^\circ$

The solidity for all tests was 1.5.

Wake measurements were made by means of a 2-inch 26-tube total-pressure rake located at midspan about 1 chord downstream of one of the center blades. These wake measurements were used to compute momentum-loss coefficients C_{w_1}. The approximate method of reference 8 was used for this computation since, for isolated airfoils, drag coefficients as determined by this method and momentum-loss coefficients are synonymous.

Additional assumptions required in order to apply this method to a cascade were that the downstream conditions be free-stream conditions and that the static pressure at the rake be equal to the static pressure far downstream. Momentum-loss coefficients calculated by this method were then based on the inlet dynamic pressure. Hence,

$$C_{w_1} = F_c \int_0^w \frac{P_w - P_e}{q_1 c} \, dw$$

where P_e is the discharge free-stream total pressure and F_c is the ratio of the momentum-loss coefficient to the total-pressure-loss coefficient.

It is the opinion of the authors that the conversion of total-pressure loss to momentum loss may be unnecessary. Since the spacing between blade rows in compressors does not vary appreciably, any variation in total-pressure loss with downstream station due to mixing is probably small. Hence, directly presenting pressure-loss coefficients appears to be justifiable. Also, if the loss coefficient is presented in terms of total-pressure loss, the use of the cascade data for loss estimation for compressor design and off-design calculations is facilitated.

The turning angles presented are the average of four downstream flow-angle measurements made outside the blade wakes in several blade gaps at midspan. For the first two of the aforementioned test conditions, schlieren photographs were taken in addition to the other measurements.

At each condition, tests were made for a range of Mach number up to choking. Reynolds numbers varied from about 6×10^5 at $M = 0.30$ to above 1.5×10^6 at the highest Mach numbers.

PRESENTATION OF DATA

The pressure distributions, expressed in terms of the pressure coefficient S, are presented in figures 7 to 10 for each of the four test configurations over the test Mach number range. The maximum surface Mach numbers and S_{cr} values are indicated. The variations in turning angle θ, momentum-loss coefficient C_{w_1}, and pressure-rise coefficient $\left(\text{expressed as } \frac{p_2 - p_1}{q_1}\right)$ with Mach number for the tests are presented in figures 11 to 14. Since there is some blockage caused by the insertion

of the rake for momentum-loss-coefficient measurements, the pressure-rise coefficients with and without the rake in place are presented. No large differences between the two were noted. The dashed curves correspond to the pressure rise that would occur in the two-dimensional condition if the effect of blade-wake blockage is approximated. The schlieren photographs taken for $\beta = 26.9^\circ$ and $\alpha = 21.5^\circ$ and for $\beta = 30.0^\circ$ and $\alpha = 24.6^\circ$ are presented in figures 15 and 16.

Since the schlieren photographs had to be taken using glass side walls, the tests were effectively solid-wall cascade tests. Since the blade pressure-tap leads would tend to obscure part of the flow field, no pressure distributions were taken for the tests with the glass side walls. To indicate to what extent the schlieren photographs are applicable to the measured pressure distributions taken using porous side walls, a comparison of the variation in θ, C_{w_1}, and $\frac{p_2 - p_1}{q_1}$ with inlet Mach number for both porous-wall and solid-wall tests is presented in figure 17. The solid-wall turning angles were generally from 0.4° to slightly over 1° greater than the porous-wall data. The C_{w_1} agreement was excellent. The side-wall boundary-layer growth for the solid-wall tests invariably resulted in lower pressure rises than occurred in the porous-wall tests, with the greatest differences naturally occurring at the higher Mach numbers. Although the difference in pressure rise for the solid- and porous-wall data presented herein has not appreciably affected turning angle and drag coefficient, it could influence surface Mach numbers in the rearward portion of the blade where many of the tests show a second velocity peak. Hence, in discussing the schlieren photographs in conjunction with the porous-wall pressure distributions, it should be realized that the local Mach numbers which actually exist in the solid-wall tests near the rear of the blade may be somewhat higher than those presented for the porous-wall pressure distributions. The order of magnitude of this difference in surface Mach number is shown in figure 18 for pressure distributions corresponding to $\beta = 26.9^\circ$ and $\alpha = 21.5^\circ$ at $M_1 \approx 0.66$. The variation in pressure rise was accomplished by altering the amount of porous-wall suction. Peak rearward surface Mach numbers increased from 0.93 to 1.00 as $\frac{p_2 - p_1}{q_1}$ was decreased from 0.185 to 0.115. The momentum-loss coefficient increased slightly with increasing pressure rise.

A comparison between a low-speed pressure distribution estimated by the method of Erwin and Yacobi (ref. 4) and the measured suction-surface pressure distribution for $\beta = 26.9^\circ$ and $\alpha = 21.5^\circ$ is presented in figure 19 and discussed in the appendix. A comparison between measured high-speed pressure distributions and those obtained from an extrapolation of measured low-speed pressure distributions for all four cascade

test conditions is presented in figure 20 and is also discussed in the appendix. The effect of pressure rise across the cascade on turning angle and momentum-loss coefficient is indicated in figure 21 for $\beta = 34.1^\circ$ and $\alpha = 25.0^\circ$ at $M_1 = 0.65$ and $\beta = 34.1^\circ$ and $\alpha = 26.5^\circ$ at $M_1 = 0.63$. The variation in momentum-loss coefficient with surface pressure-rise coefficient (termed the C-factor in ref. 9) is presented in figure 22.

DISCUSSION

Test Results at $\beta = 26.9^\circ$, Corresponding to Hub Section of Transonic Rotor of Reference 2

The low-speed design angle of attack is 19.4° if the design angle-of-attack conditions for the A_{10} and A_2I_{8b} conditions in references 1 and 3 are interpolated. At $\beta = 26.9$, the higher angle-of-attack condition, namely $\alpha = 21.5^\circ$, was tested because, as mentioned previously, high-speed cascade tests have indicated that, for cascades which have contraction ratios less than 1.00, the angle of attack for minimum drag increases with inlet Mach number. Based on an interpolation of the data in references 1 and 3, $\theta_d = 39^\circ$. For $\frac{d\theta}{d\alpha} = 1.0$ the turning angle at $\alpha = 21.5^\circ$ should then be 41.1°. The turning angles obtained in the high-speed cascade tunnel agreed quite well with this value over the low loss range of operation where θ varied from 40.0° to 40.9°. (See fig. 11.) A rapid rise in momentum-loss coefficient occurred for inlet Mach numbers above 0.70. At $M_1 = 0.750$ (fig. 7(f)) the maximum measured surface Mach number was 1.24 at the 70-percent-chord station and the peak surface Mach number in the nose region was 1.03. An examination of the corresponding schlieren photographs (fig. 15) should indicate which of the two pressure rises along the suction surface is primarily responsible for the increase in loss. There appeared to be no substantial increase in boundary-layer thickness along the first 70 percent of the blade for the entire test Mach number range. Hence, the local small shocks which are visible at the higher inlet Mach numbers are not detrimental to the blade performance. Therefore, the high drag at inlet Mach numbers above 0.70 must result from shock-induced boundary-layer separation behind the shock which occurs at approximately the 70-percent point. The appreciable curvature just behind the shock is conducive to flow separation. Also, there is more likelihood of flow separation because this shock occurred in the rearward portion of the blade where the boundary layer is thicker.

It should be pointed out that, even at the lower subsonic Mach numbers, the schlieren photographs indicated that the flow did not follow the suction-surface curvature in the last 10 percent of the blade. The low C_{w_1} values, however, indicate that the degree of separation is no worse than for any other highly cambered section.

The development of a more nearly optimum blade section for the hub-type conditions under investigation in order to increase the level of inlet Mach number for efficient operation above $M_1 = 0.70$ will require the reduction and possibly the elimination of the second velocity peak which occurred in the suction-surface pressure distributions shown in figure 7. This result can be achieved through a reduction of the curvature in the rearward portion of the blade by moving some of the rearward mean-line loading to the middle and more forward portion of the blade. The loading shift could be attained by using the A_{10} or a circular-arc mean line in conjunction with the T1 thickness distribution. If the rearward curvature is still not reduced sufficiently, a further reduction may be effected by using a thickness distribution in which the maximum thickness is not as far back as that of the T1 thickness distribution and/or possibly by using a thicker trailing-edge radius. The double circular-arc blade section might prove to be quite desirable for such hub conditions. However, some care must be taken to avoid raising the Mach numbers and surface curvature in the forward portion to such a level that strong shocks form, resulting in shock-induced flow separation in the forward position.

For the hub-type conditions of inlet angle, turning angle, and solidity herein investigated, it appears that, for a maximum thickness of 8 percent and Mach numbers above 0.70, supersonic surface velocities are inevitable. The only way that efficient performance can be obtained for such conditions is to keep surface curvature to a minimum in the region where a surface shock will occur while, of course, attempting to minimize surface Mach numbers. Unfortunately, the limits for various combinations of shock strength, blade-surface curvature, and boundary-layer thickness just ahead of the shock have not as yet been established. The establishment of such limits will permit a determination of the type of blading that is most effective for transonic compressor hub sections. A considerable amount of fundamental research on this problem is needed.

In summary, these tests indicated that high-speed turning angles can be effectively estimated from low-speed cascade test results. They indicate that turning angles of approximately 40° at an inlet angle of 26.9° can be accomplished without severe loss for inlet Mach numbers up to $M_1 = 0.70$ by using the type of blade mean line and thickness distribution herein described. For efficient operation at inlet Mach numbers much above 0.70 for an 8-percent-thick blade at this cascade condition, some alteration of the distribution of surface curvature is

necessary either by suitably altering the thickness distribution or by using a mean line which shifts some of the rearward loading toward the middle of the blade.

Effect of More Forward Location of Peak Surface Velocities

In order to obtain information regarding the effect of raising surface Mach numbers in the forward portion of the blade where surface curvature is less, while reducing surface Mach numbers in the highly curved rearward region where the strong shock had produced flow separation, the blades were tested at a higher inlet angle and a higher angle of attack, namely, $\beta = 30^\circ$ and $\alpha = 24.6^\circ$.

The minimum momentum-loss coefficient was slightly higher than that obtained at the lower angle of attack. (See figs. 11 and 12.) The inlet Mach number for rapid drag rise increased from 0.70 for the lower inlet-angle condition to over 0.75 for this test condition. A comparison of the pressure distributions at $\beta = 26.9^\circ$ and $\beta = 30.0^\circ$ at $M = 0.708$ and $M = 0.751$, respectively (figs. 7(e) and 8(d)), indicated no increase in momentum-loss coefficient for the higher angle-of-attack condition even though the maximum local pressure coefficient indicated that a peak local Mach number of 1.18 existed in the forward portion of the blade at the higher angle of attack. Hence, shocks of this strength in the forward portion of the blade where the curvature is low and the boundary layer is thin will not adversely affect blade performance.

The schlieren photographs corresponding to this inlet-angle condition are presented in figure 16. No appreciable increase in boundary-layer thickness after the forward-region shock waves was noted for inlet Mach numbers up to 0.80 for the middle blade shown in the schlieren photographs (figs. 16(a) to 16(g)). The middle blade is stipulated because at $M_1 = 0.80$ (fig. 16(g)), the shocks are not uniform from blade to blade. Since the pressure distribution corresponding to this inlet Mach number of 0.799 (fig. 8(e)) indicated a maximum local Mach number near the nose of approximately 1.26, it appears that Mach numbers this high can be tolerated in the forward portion of the blade.

At $M_1 = 0.80$, most of the flow separation occurs after the second series of shocks which occur at approximately the 70-percent-chord point. The pressure distribution indicates a maximum local Mach number of approximately 1.25 at the 70-percent-chord point. Separation occurred here for the same Mach number level for which no appreciable separation was noted in the forward portion of the blade because (1) the approach boundary layer was thicker in the rearward portion of the blade, (2) the blade-surface curvature was more severe there, and (3) the amount of surface-pressure recovery was greater in this rearward region.

The schlieren photograph for $M = 0.82$ (fig. 16(h)) indicated a significant increase in boundary-layer thickness behind the first shock pattern, which is, of course, characteristic of impending flow separation. Hence, the surface Mach number of 1.26 near the leading edge for the $M_1 = 0.80$ test is quite close to the separation limit for the curvature conditions which existed in the forward portion of the blade.

Effect of Increase in Pressure-Rise Coefficient

To investigate this blading under higher pressure-rise conditions, tests were conducted at an inlet angle of 34.1° at angles of attack of 25° and 26.5°. Some increase in momentum loss even at low Mach numbers was evident for these higher pressure-rise tests. For example, at $M_1 = 0.5$ and $\beta = 34.1^\circ$, C_{w_1} was 0.022 and 0.024 for $\alpha = 25^\circ$ and $\alpha = 26.5^\circ$, respectively, (figs. 13 and 14), whereas at the lower pressure-rise conditions (figs. 11 and 12), C_{w_1} values at $M_1 = 0.5$ ranged from 0.015 to 0.017.

For $\beta = 34.1^\circ$ and $\alpha = 25^\circ$, C_{w_1} began to rise gradually above $M_1 = 0.50$ and increased rapidly above 0.84. The trend of C_{w_1} with Mach number was similar to that indicated by the data for $\beta = 30^\circ$ and $\alpha = 24.6^\circ$ in figure 12. Both conditions showed C_{w_1} to be approximately 0.03 at $M_1 = 0.80$ with the higher inlet-angle condition having a pressure-rise coefficient $\frac{p_2 - p_1}{q_1}$ of 0.38 compared with 0.27 for the $\beta = 30^\circ$ condition.

At $M_1 = 0.805$, $\beta = 34.1^\circ$, and $\alpha = 25^\circ$, the blading exhibited a maximum local Mach number near the nose of 1.27 (fig. 9(d)). A comparison of this pressure distribution with that at $M_1 = 0.799$, $\beta = 30^\circ$, and $\alpha = 24.6^\circ$ (fig. 8(e)) indicated that both conditions had approximately the same peak local Mach numbers and the same moderately high momentum-loss coefficients. The higher inlet-angle condition, however, has a much lower local Mach number at the 70-percent-chord point as well as a lower pressure recovery from the 70-percent-chord point to the trailing edge. The major difference between the two conditions in the forward region is that the test at the higher inlet angle actually experienced a more severe pressure recovery from the 10-percent to the 30-percent point. Evidently, at the higher inlet angle the flow separation which must occur behind the shock pattern for C_{w_1} to be as high as 0.03 was caused by the increased pressure recovery which occurred near the leading edge for that test. Hence, as expected, for the same

surface curvature the limiting value of local Mach number to avoid separation in the leading-edge region is dependent on the pressure-rise condition which the flow field imposes.

At surface Mach numbers of about 1.27, the test data at $\beta = 34.1^\circ$ indicated a somewhat different result at $\alpha = 26.5^\circ$ (fig. 10) from that which was observed at $\alpha = 25^\circ$ (fig. 9). The higher angle-of-attack condition had a C_{w_1} of 0.026 when $M_m = 1.26$ (fig. 10(c)) compared to a C_{w_1} of 0.031 at $M_m = 1.27$ for the lower angle-of-attack condition (fig. 9(d)). Evidently, low C_{w_1} values are obtainable for peak local Mach numbers as high as 1.26 providing that this peak Mach number occurs very close to the leading edge (near the 2.5-percent-chord point).

The major differences between these two conditions are: (1) the lower loss condition at the higher angle of attack has its shock closer to the leading edge and, hence, its approach boundary layer will be thinner; and (2) both the pressure-recovery gradient $\frac{dp}{dc}$ and the amount of the pressure recovery are greater at the higher α condition whereas the surface Mach numbers over the rear 60 percent of the blade are lower. Apparently, having the pressure recovery occur nearer the leading edge where boundary-layer thickness is less may be the main reason for the lower loss associated with the higher angle-of-attack test.

There was a considerable increase in C_{w_1} of from 0.026 to 0.032 when the peak local Mach number near the leading edge was increased from 1.26 to 1.28. (See figs. 10(d) and 10(e).) Hence, it appears that $M_m = 1.26$ is close to the separation limit for the curvature conditions which existed near the leading edge.

Effect of Mach Number and Pressure Rise on Turning Angle

The data of figures 11 to 14 show only a slight variation in turning angle (at most, about $\pm 0.5^\circ$) with Mach number for momentum-loss coefficients up to approximately 0.03. To determine the effect of variation in back pressure produced by varying the amount of porous-wall suction, typical conditions were examined at the same inlet Mach number with varying amounts of porous-wall suction. Figure 21 shows the variation in turning angle and C_{w_1} with $\frac{p_2 - p_1}{q_1}$ for $\beta = 34.1^\circ$ and $\alpha = 25.0^\circ$ at $M_1 = 0.65$ and for $\beta = 34.1^\circ$ and $\alpha = 26.5^\circ$ at $M_1 = 0.63$. An increase in $\frac{p_2 - p_1}{q_1}$ of approximately 28 percent resulted in a decrease in turning angle of 0.4° for $\alpha = 26.5^\circ$. An increase in $\frac{p_2 - p_1}{q_1}$ of approximately 33 percent corresponded to a decrease in turning angle of 1.5° for $\alpha = 25.0^\circ$. For both angles of attack, C_{w_1} increased somewhat with increasing $\frac{p_2 - p_1}{q_1}$.

Comparison of Variation in Momentum-Loss Coefficient With Surface Pressure-Rise Coefficient

The measured pressure-distribution data were used to compute the surface pressure-rise coefficient. It is defined as the ratio of the maximum pressure rise on the blade suction surface to the difference between the total and static pressure at the point of maximum surface velocity and is called the C-factor. The variation in C_{w_1} with C-factor for the four cascade configurations tested is presented in figure 22. The limit value of the C-factor for low momentum loss ranged from 0.61 to 0.68 for three of the four conditions and was 0.54 for the other. These values were considerably below the 0.75 to 0.80 values obtained from low-speed cascade data in reference 9.

The boundary-layer development along the blade for these tests has been complicated by shock boundary-layer interaction effects which, of course, did not occur in the low-speed tests. Also, there will generally be some boundary-layer thickening behind surface shock waves. These boundary layers cannot tolerate as severe a pressure recovery as could a thinner boundary layer, and, hence, separation occurs at lower C-factors than in the low-speed tests.

One possible explanation that the test with $\beta = 26.9^\circ$ and $\alpha = 21.5^\circ$ showed a lower level of limiting C-factor than the other three test conditions is that this was the only condition at which flow separation was almost entirely governed by the second pressure recovery. It represented the most confined passage condition and even at the high momentum-loss condition, $M_1 = 0.750$ (fig. 7(f)), it had only very slightly supersonic velocities in the nose ($M_7 = 1.03$) compared with $M_7 = 1.24$ at the 70-percent chordwise station. It is reasonable to presume that, as the location of a given pressure recovery shifts rearward, the amount of pressure recovery possible without separation will decrease since both the adverse pressure gradient and the thickness of the initial boundary layer will increase.

It appears that, in the use of any simple loading-limit parameter, such as the C-factor, it is necessary to make certain that the surface pressure distributions are not far different from those used to establish such limits. The successful use of such a loading-limit parameter will require analysis of sufficient data to establish limiting values for typical examples of differently shaped pressure distributions since it has been shown that C-factor limits will vary with significant changes in surface-pressure-distribution shape which can influence the boundary-layer development.

CONCLUSIONS

The high-speed cascade tests of a T1-(18A_6I_{4b})08 blade section at a solidity of 1.5 at several inlet angles ranging from 26.9° to 34.1° have indicated the following conclusions:

1. Turning angles of the order of 40° can be accomplished without severe loss for inlet Mach numbers up to 0.70 at an inlet angle of 26.9° and up to 0.75 at an inlet angle of 30.0°. At inlet angles from 30.0° to 34.1° momentum-loss coefficients of approximately 0.03 were obtained at an inlet Mach number of 0.80.

2. A surface Mach number near the nose of the blade of approximately 1.26 appeared to be close to the separation limit for the curvature conditions which existed near the leading edge.

3. High-speed turning angle can be effectively estimated from low-speed cascade test results since the variation in turning angle with inlet Mach number for momentum-loss coefficients up to approximately 0.03 is small (at most, about ±0.5).

Langley Aeronautical Laboratory,
National Advisory Committee for Aeronautics,
Langley Field, Va., June 8, 1955.

[redacted]

ESTIMATION OF BLADE-SURFACE PRESSURE DISTRIBUTIONS

Estimation of T1-$(18A_6I_{4b})$08 Blade Incompressible Suction-Surface Pressure Distribution at $\beta = 26.9^\circ$, $\alpha = 21.4^\circ$, and $\sigma = 1.5$

The method of estimating low-speed pressure distributions presented in reference 4 was used to compute the suction-surface pressure distribution for the T1-$(18A_6I_{4b})$08 blade at $\beta = 26.9^\circ$, $\alpha_d = 19.4^\circ$, and $\sigma = 1.5$. The surface pressure coefficients at $\alpha = 21.4^\circ$, which is 2.1° above design, were obtained by adding the incremental surface velocities due to angle of attack to the surface velocities for design angle of attack. The surface velocities due to angle of attack which were used were the empirical results obtained for the 65-$(12A_{10})$10 blade at $\beta = 30^\circ$ which were presented in figure 15 of reference 10.

To approximate the incremental surface velocities due to thickness for the 10-percent-thick T1 thickness distribution, the surface velocities for the following thickness distributions as obtained from reference 11 were used for various portions of the blade:

Percent chord	Thickness distribution from which incremental velocities due to thickness were obtained
0 to 25	A 7-percent-thick 65-series thickness distribution
25 to 55	Incremental velocities obtained from faired curve between incremental velocities due to thickness for 0 to 25 percent and 55 to 100 percent
55 to 100	NACA 63-010 reversed

The surface velocities due to thickness for the 8-percent-thick blade were obtained by multiplying the velocities for the 10-percent-thick blade by 0.8. It should be pointed out that the incremental velocities due to thickness are considerably less than those due to camber, for cambers of the order of 1.8. Hence, the rather approximate method of obtaining the effects of thickness on surface velocity was considered adequate.

The incremental surface velocities due to camber for $C_{l_o} = 1.8$ with an A_6I_{4b} mean line were also obtained from reference 11. The incremental velocities of the $a = 1.0$ mean line were added to those of the reversed $a = 0.2$ in the proportions of 60 percent and 40 percent, respectively, for $C_{l_o} = 1.8$ for each of the component types of mean line.

The cascade interference factors were obtained for the AB and CF regions as indicated in reference 4, and those for the BC region were obtained from a faired curve between the factors for the AB and CF regions. The resulting variation in interference factor F with chordwise position is as follows:

Station, percent chord	Interference factor, F	Station, percent chord	Interference factor, F
0	0.683	20	0.510
5	.680	25	.432
10	.666	30	.402
15	.625	35 to 100	.391

A comparison of estimated incompressible and measured suction-surface pressure distribution at $M_1 = 0.305$ is presented in figure 19. It may be seen that fairly good agreement was obtained in the forward portion of the blade (the first 60 percent of the blade). In the 60- to 90-percent region, measured surface velocities were higher than estimated. These higher surface velocities may result because the curvature of this blade in this region is considerably greater than that of the blading considered in reference 4 and, hence, the velocity which typifies the free-stream flow field for this region may be higher than the average velocity obtained from one-dimensional area considerations.

Extrapolation of Pressure Distributions From Low to High Speed

The low-speed pressure distributions at $M_1 = 0.30$ were used with the extrapolation procedure described in reference 1 to obtain predicted high-speed pressure distributions at approximately $M_1 = 0.70$. The comparisons between measured and estimated suction-surface pressure coefficients are presented in figure 20. In general, good agreement was obtained between estimated and measured values. The largest discrepancy occurred at the lowest inlet-angle condition (fig. 20(a)). The extrapolation procedure was considered to be fairly effective in estimating high-speed pressure coefficients from low-speed pressure distributions for conditions of low inlet angle, high solidity, and high camber.

REFERENCES

1. Erwin, John R., Savage, Melvyn, and Emery, James C.: Two-Dimensional Low-Speed Cascade Investigation of NACA Compressor Blade Sections Having a Systematic Variation in Mean-Line Loading. NACA RM L53I30b, 1953.

2. Savage, Melvyn, and Felix, A. Richard: Investigation of a High-Performance Axial-Flow Compressor Transonic Inlet Rotor Designed for 37.5 Pounds Per Second Per Square Foot of Frontal Area - Aerodynamic Design and Overall Performance. NACA RM L55A05, 1955.

3. Herrig, L. Joseph, Emery, James C., and Erwin, John R.: Systematic Two-Dimensional Cascade Tests of NACA 65-Series Compressor Blades at Low Speeds. NACA RM L51G31, 1951.

4. Erwin, John R., and Yacobi, Laura A.: Method of Estimating the Incompressible-Flow Pressure Distribution of Compressor Blade Sections at Design Angle of Attack. NACA RM L53F17, 1953.

5. Herrig, L. Joseph, Emery, James C., and Erwin, John R.: Effect of Section Thickness and Trailing-Edge Radius on the Performance of NACA 65-Series Compressor Blades in Cascade at Low Speeds. NACA RM L51J16, 1951.

6. Lieblein, Seymour, Lewis, George W., Jr., and Sandercock, Donald M.: Experimental Investigation of an Axial-Flow Compressor Inlet Stage Operating at Transonic Relative Inlet Mach Numbers. I - Over-All Performance of Stage With Transonic Rotor and Subsonic Stators up to Rotor Relative Inlet Mach Number of 1.1. NACA RM E52A24, 1952.

7. Lewis, George W., Jr.: Experimental Investigation of Axial-Flow Compressor Inlet Stage Operating at Transonic Relative Inlet Mach Numbers. II - Blade-Coordinate Data. NACA RM E52C27, 1952.

8. Heaslet, Max A.: Theoretical Investigation of Methods for Computing Drag From Wake Surveys at High Subsonic Speeds. NACA WR-1, 1945. (Formerly NACA ARR 5C21.)

9. Savage, Melvyn: Analysis of Aerodynamic Blade-Loading-Limit Parameters for NACA 65-$(C_{l_0}A_{10})$10 Compressor-Blade Sections at Low Speeds. NACA RM L54L02a, 1955.

10. Felix, A. Richard, and Emery, James C.: A Comparison of Typical National Gas Turbine Establishment and NACA Axial-Flow Compressor Blade Sections in Cascade at Low Speed. NACA RM L53B26a, 1953.

11. Abbott, Ira H., Von Doenhoff, Albert E., and Stivers, Louis S., Jr.: Summary of Airfoil Data. NACA Rep. 824, 1945. (Supersedes NACA WR L-560.)

TABLE I

COORDINATES FOR T1 THICKNESS DISTRIBUTION

HAVING 8-PERCENT MAXIMUM THICKNESS

[Stations and ordinates in percent chord]

x	y	
	Upper surface	Lower surface
0	0	0
.500	.444	-.444
.750	.537	-.537
1.250	.671	-.671
2.500	.894	-.894
5.000	1.224	-1.224
7.500	1.464	-1.464
10.000	1.664	-1.664
15.000	2.000	-2.000
20.000	2.304	-2.304
25.000	2.584	-2.584
30.000	2.824	-2.824
35.000	3.048	-3.048
40.000	3.240	-3.240
45.000	3.424	-3.424
50.000	3.608	-3.608
55.000	3.784	-3.784
60.000	3.952	-3.952
65.000	4.000	-4.000
70.000	3.896	-3.896
75.000	3.656	-3.656
80.000	3.296	-3.296
85.000	2.776	-2.776
90.000	2.168	-2.168
95.000	1.464	-1.464
100.000	0	0
R_{LE} = 0.220 R_{TE} = 0.800		

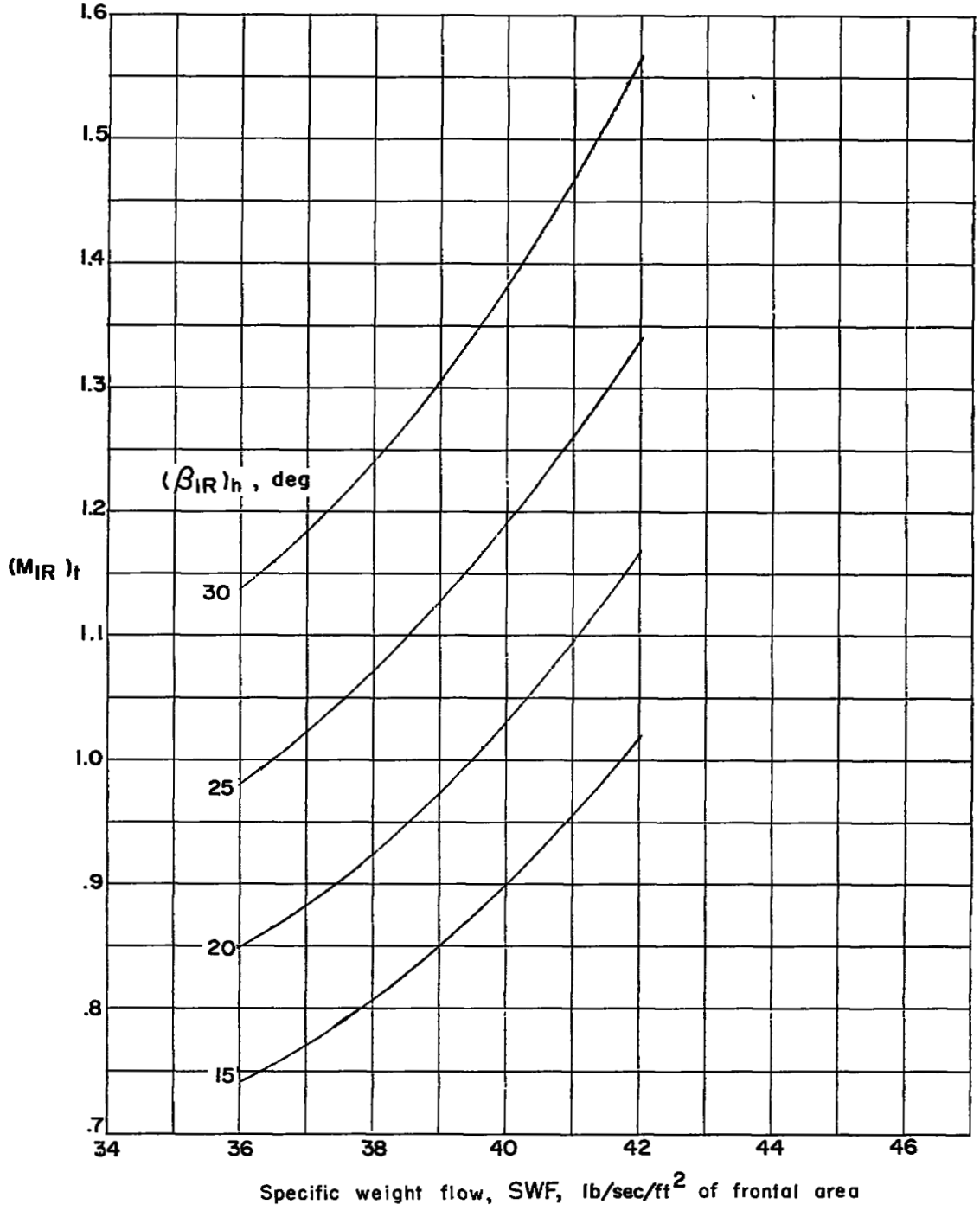

Figure 1.- Effect of specific weight flow on rotor-tip inlet Mach number for various rotor-hub inlet angles with an inlet hub-tip ratio of 0.35 and no guide vanes at standard sea-level conditions. P = 2,116 lb/sq ft and T = 518.6° R.

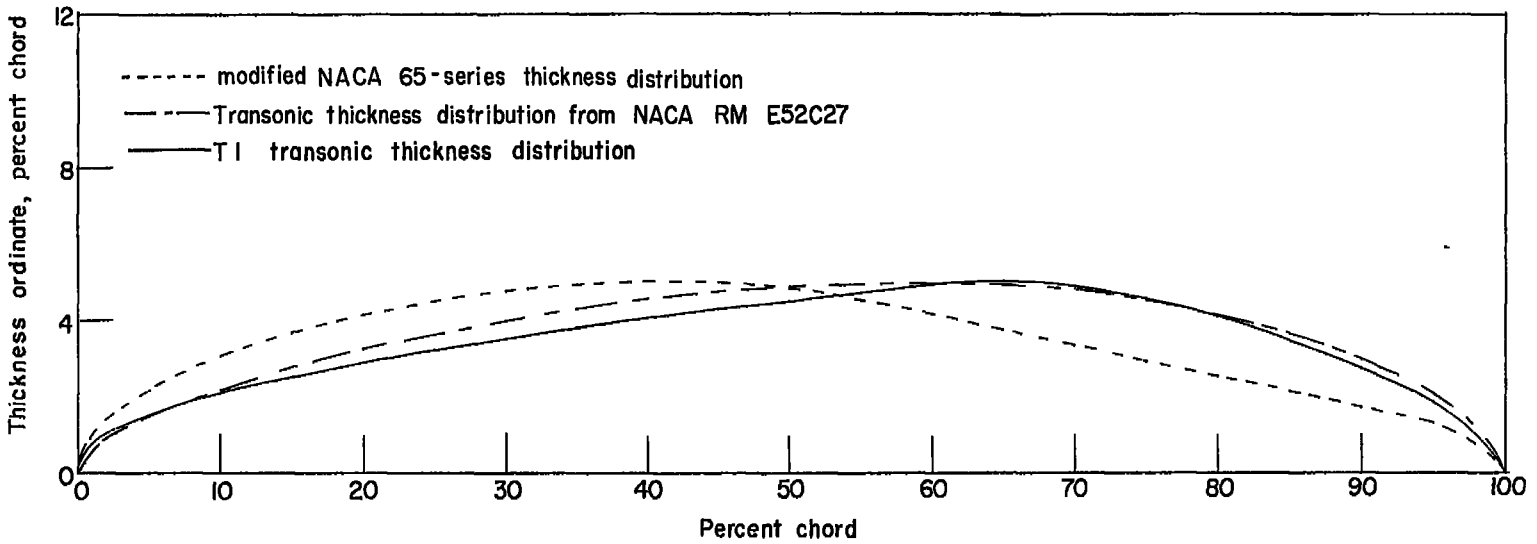

Figure 2.- Comparison of several thickness distributions for $t/c = 0.10$.

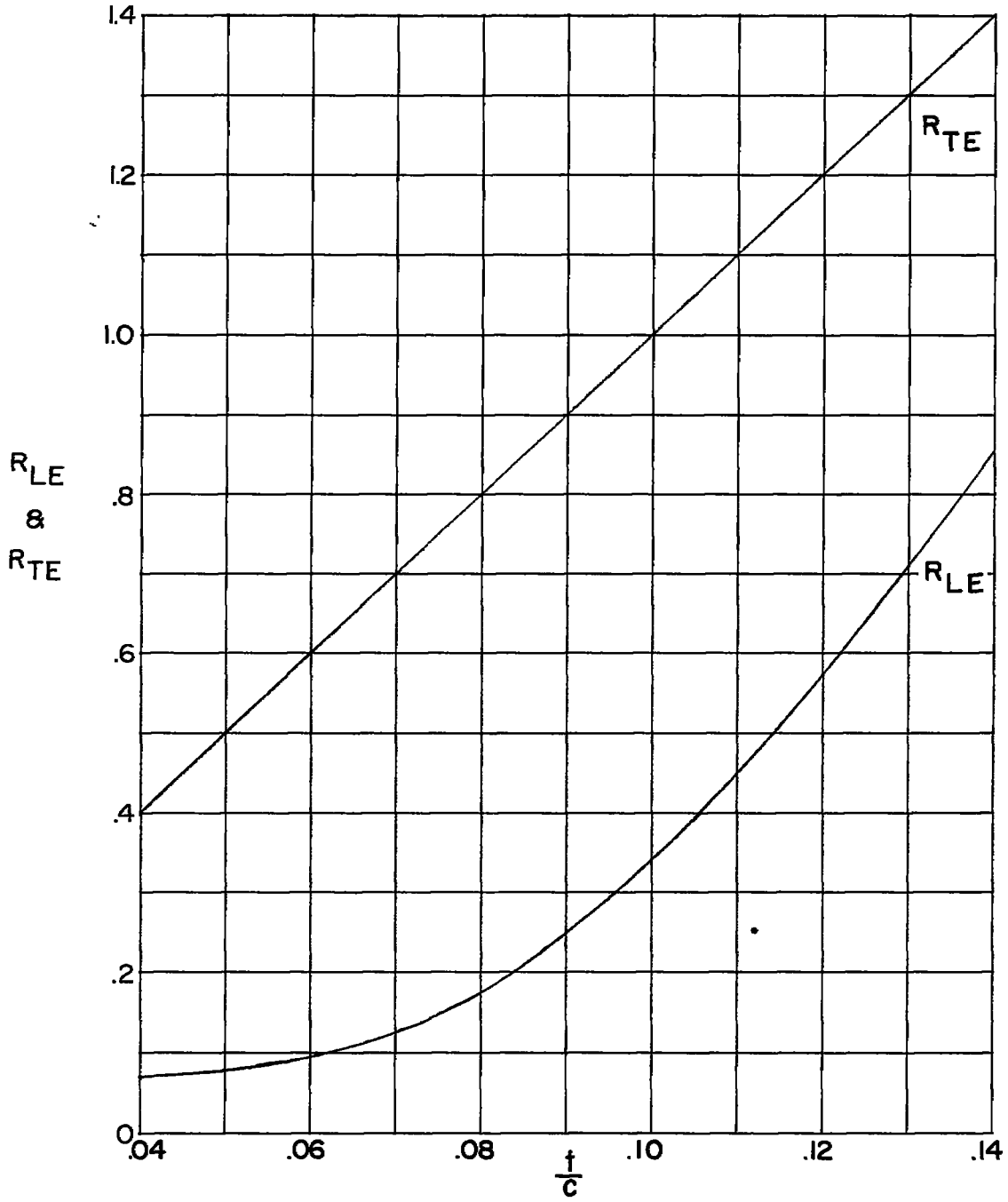

Figure 3.- Variation of leading- and trailing-edge radii with blade-section thickness for T1 thickness distribution.

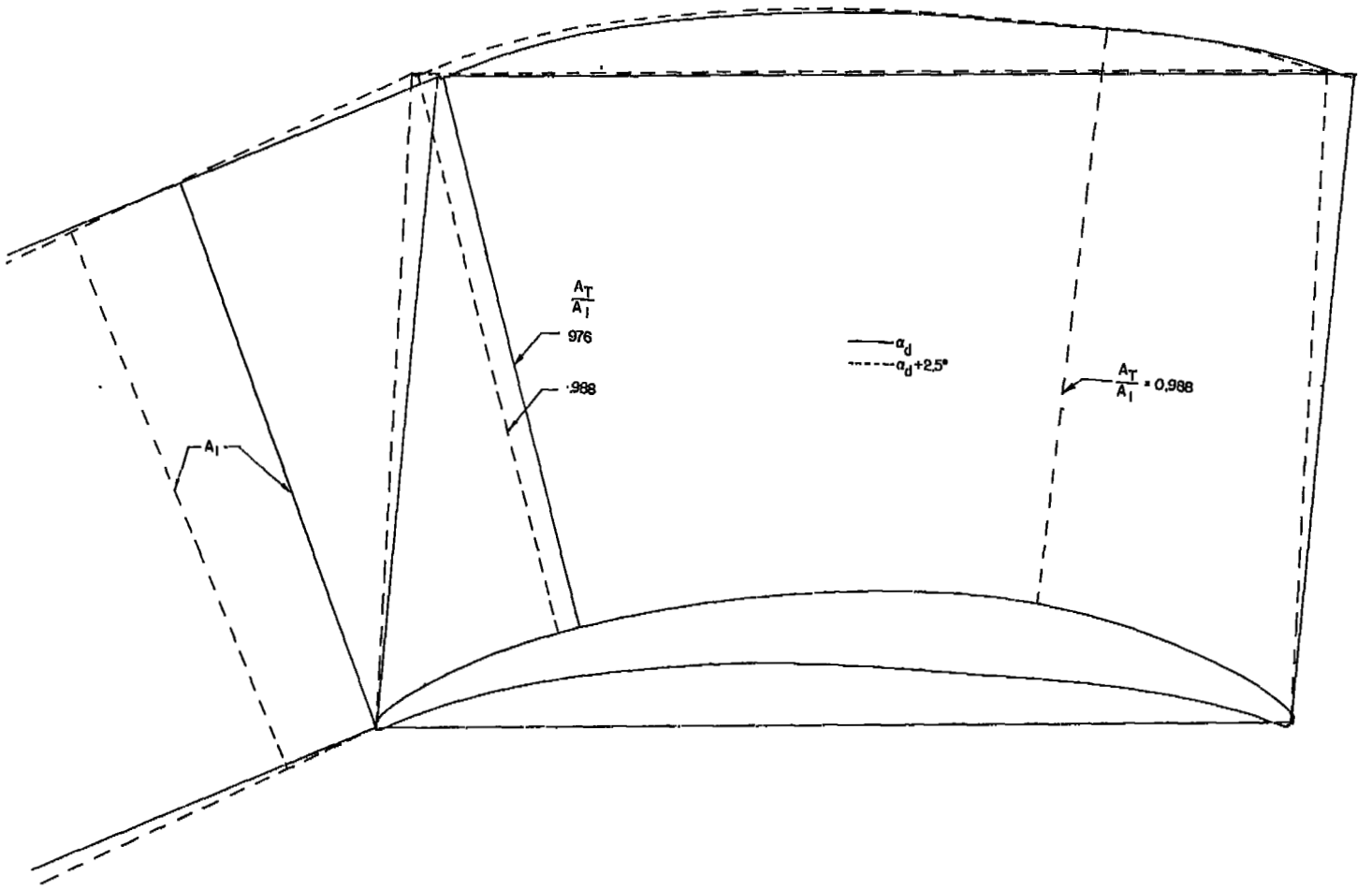

(a) T1-$\left(18A_{10}\right)$08, α_d = 20.8°.

Figure 4.- Cascade passage-area distribution at β = 26.9° and σ = 1.5 for t/c = 0.08.

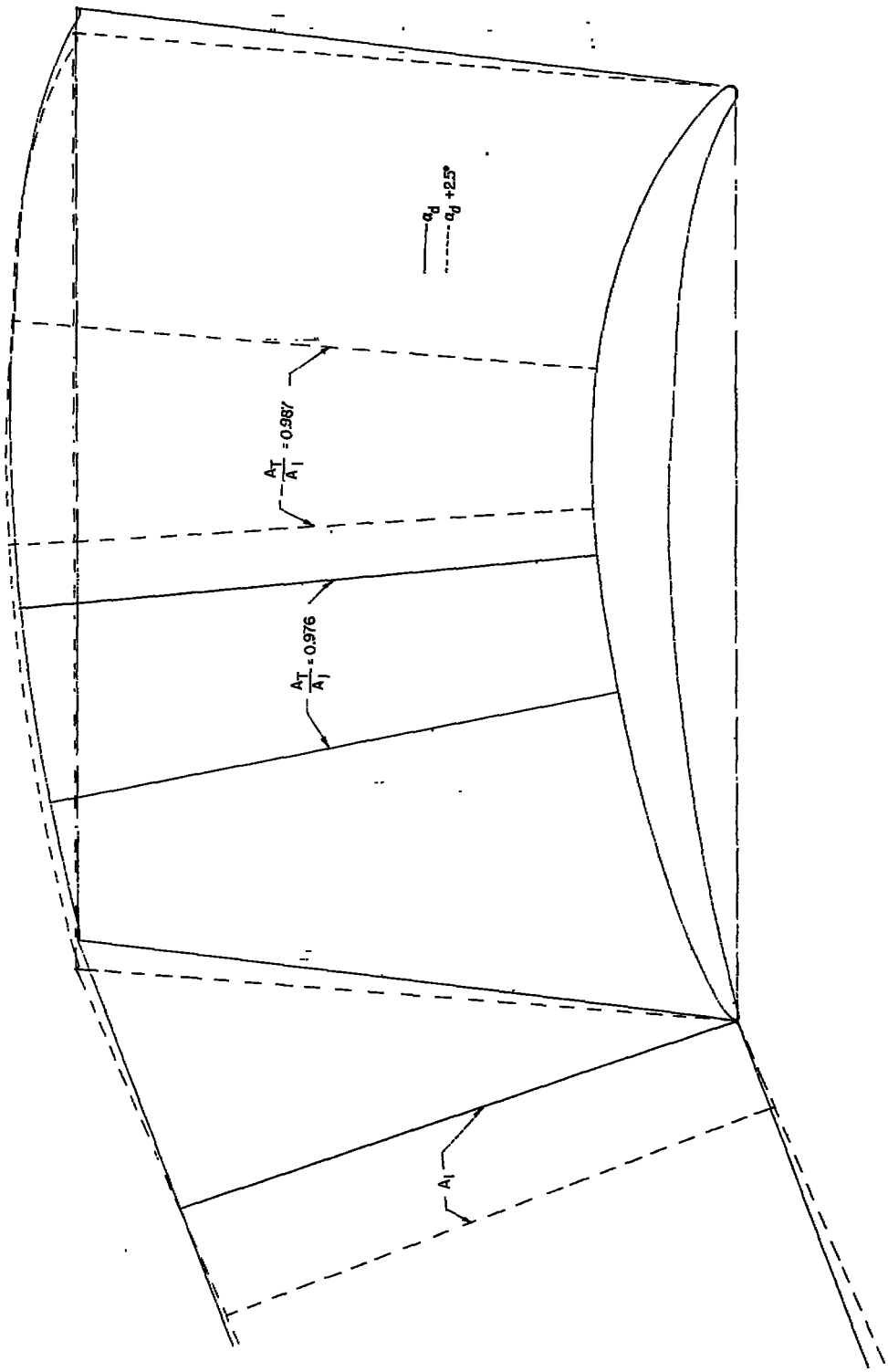

(b) $T1-\left(18A_6T_{4b}\right)08$, $\alpha_a = 19.4°$.

Figure 4.- Continued.

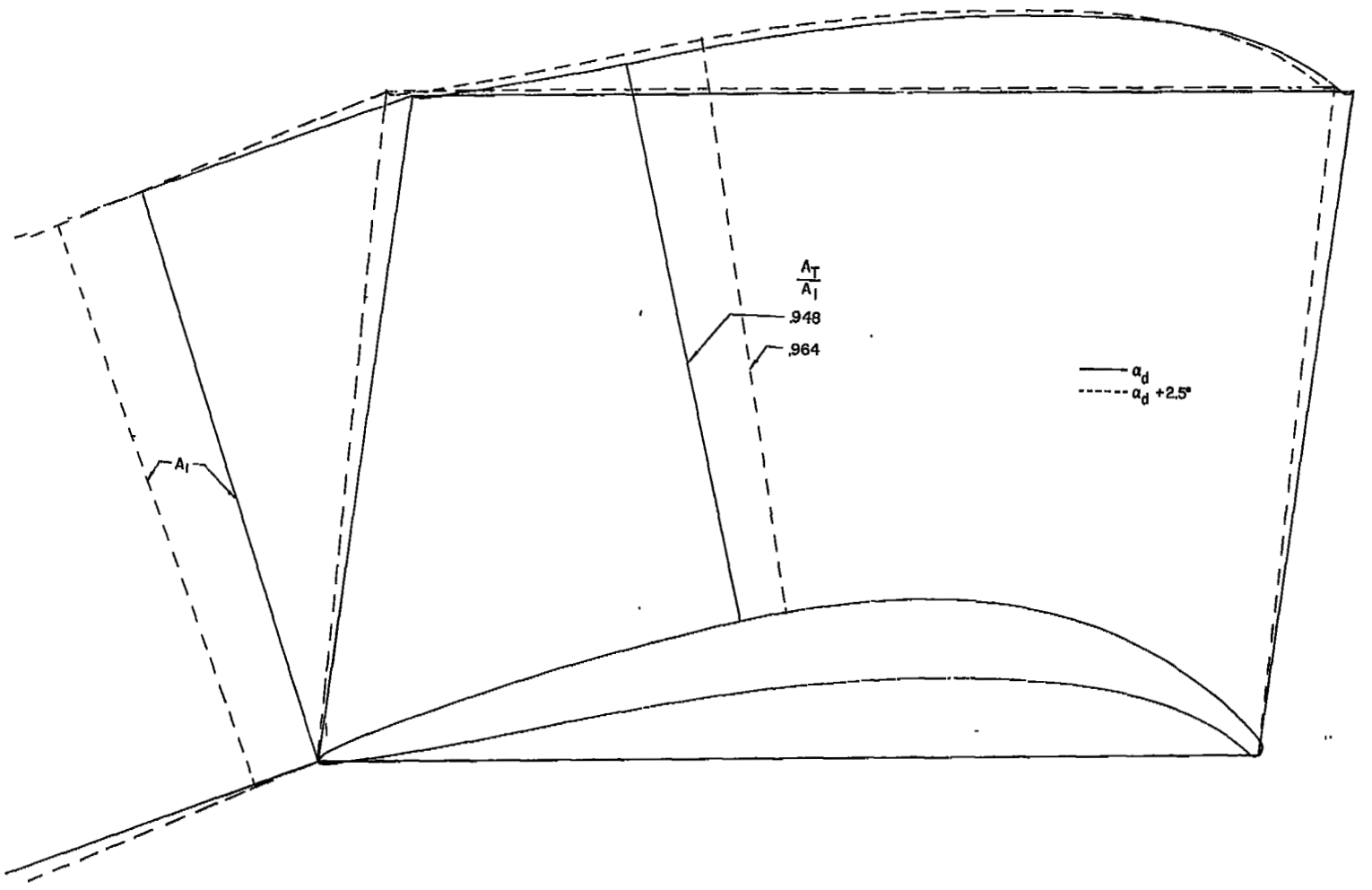

(c) T1-$\left(18A_2I_{8b}\right)$08, α_d = 18.0°.

Figure 4.- Concluded.

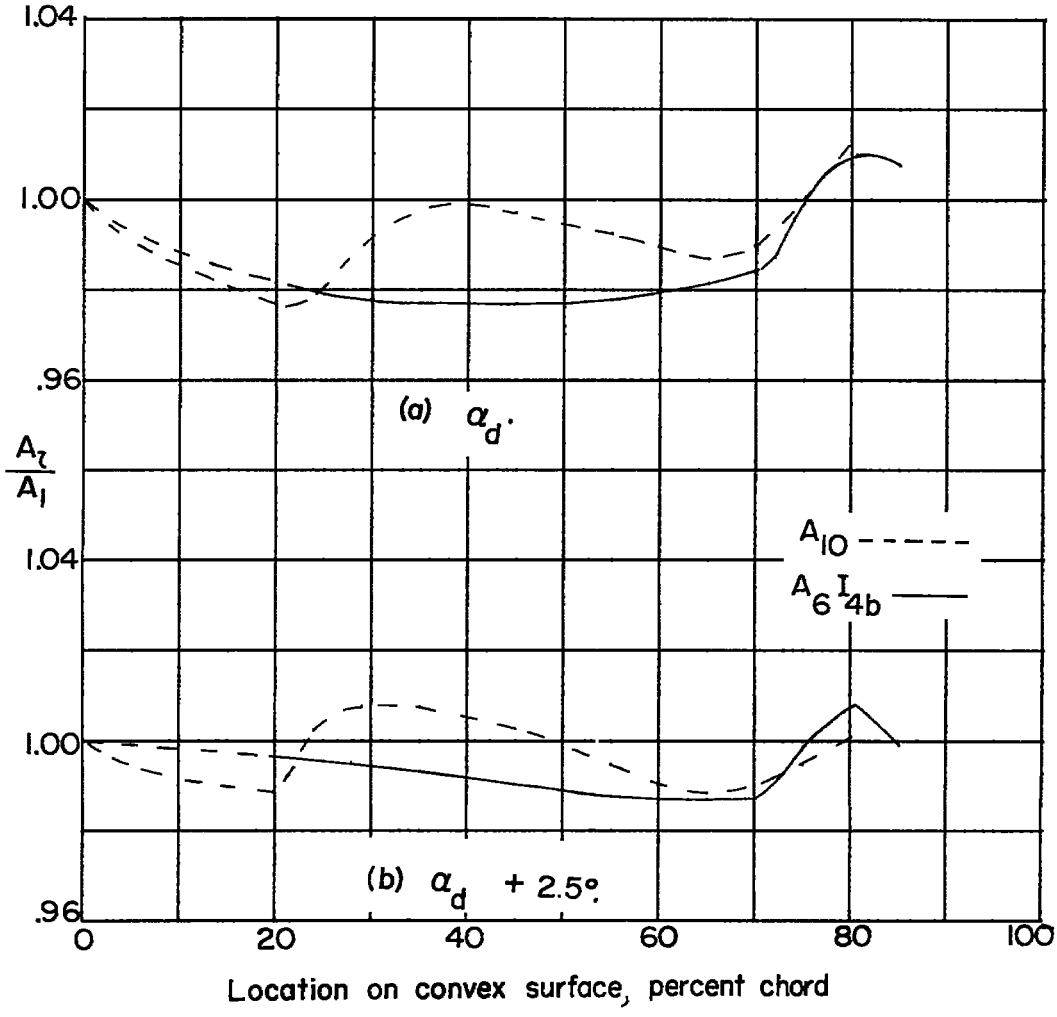

Figure 5.- Variation in passage-area distribution through cascade with mean line for blades having T1 thickness distribution, $C_{l_o} = 1.8$, and $t/c = 0.08$ at $\beta = 26.9^\circ$ and $\sigma = 1.5$.

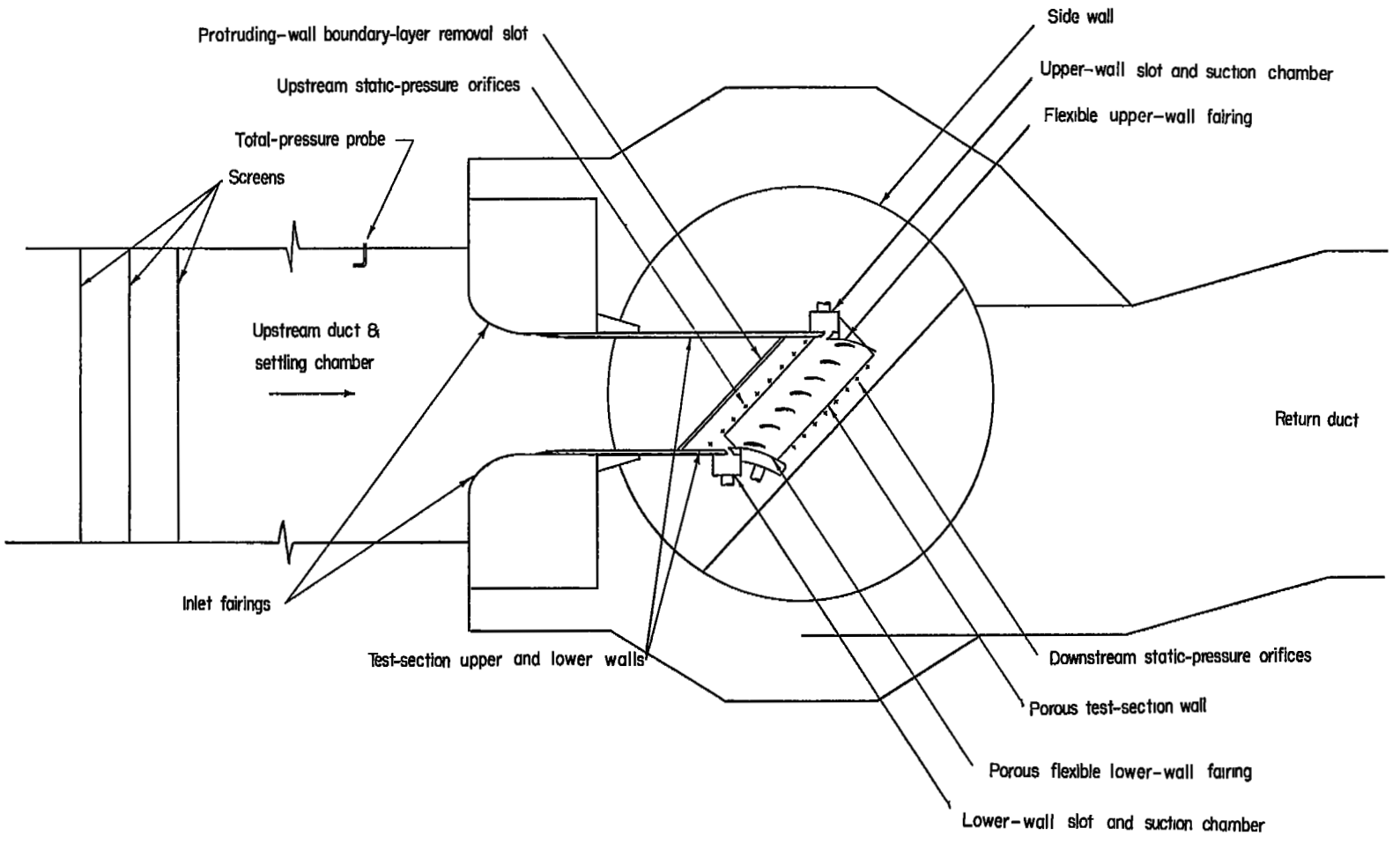

Figure 6.- Schematic diagram of 7-inch high-speed cascade tunnel.

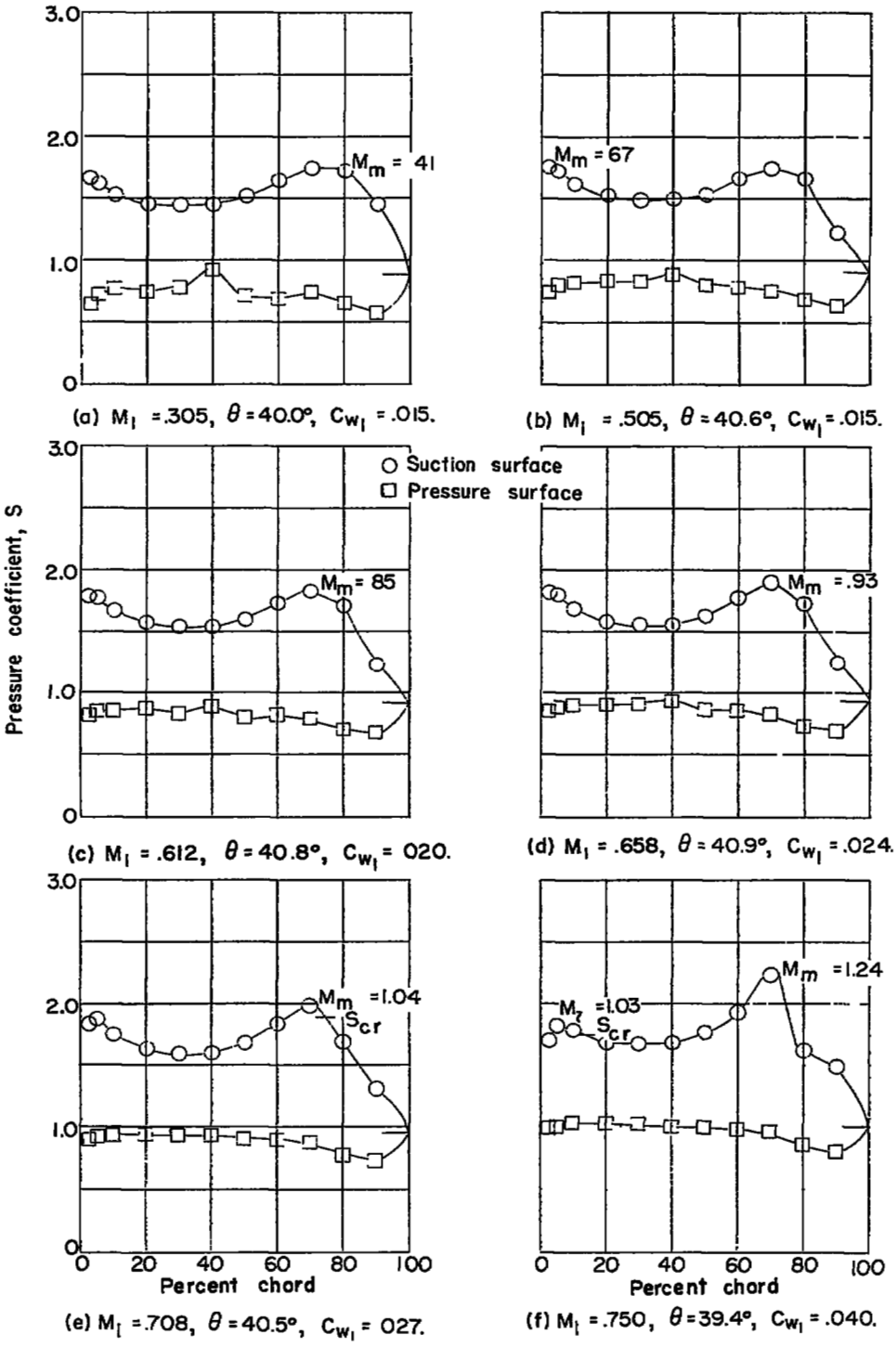

Figure 7.- Blade-surface pressure distribution and section characteristics for T1-$\left(18A_6I_{4b}\right)$08 blade at $\beta = 26.9°$, $\sigma = 1.5$, and $\alpha = 21.5°$.

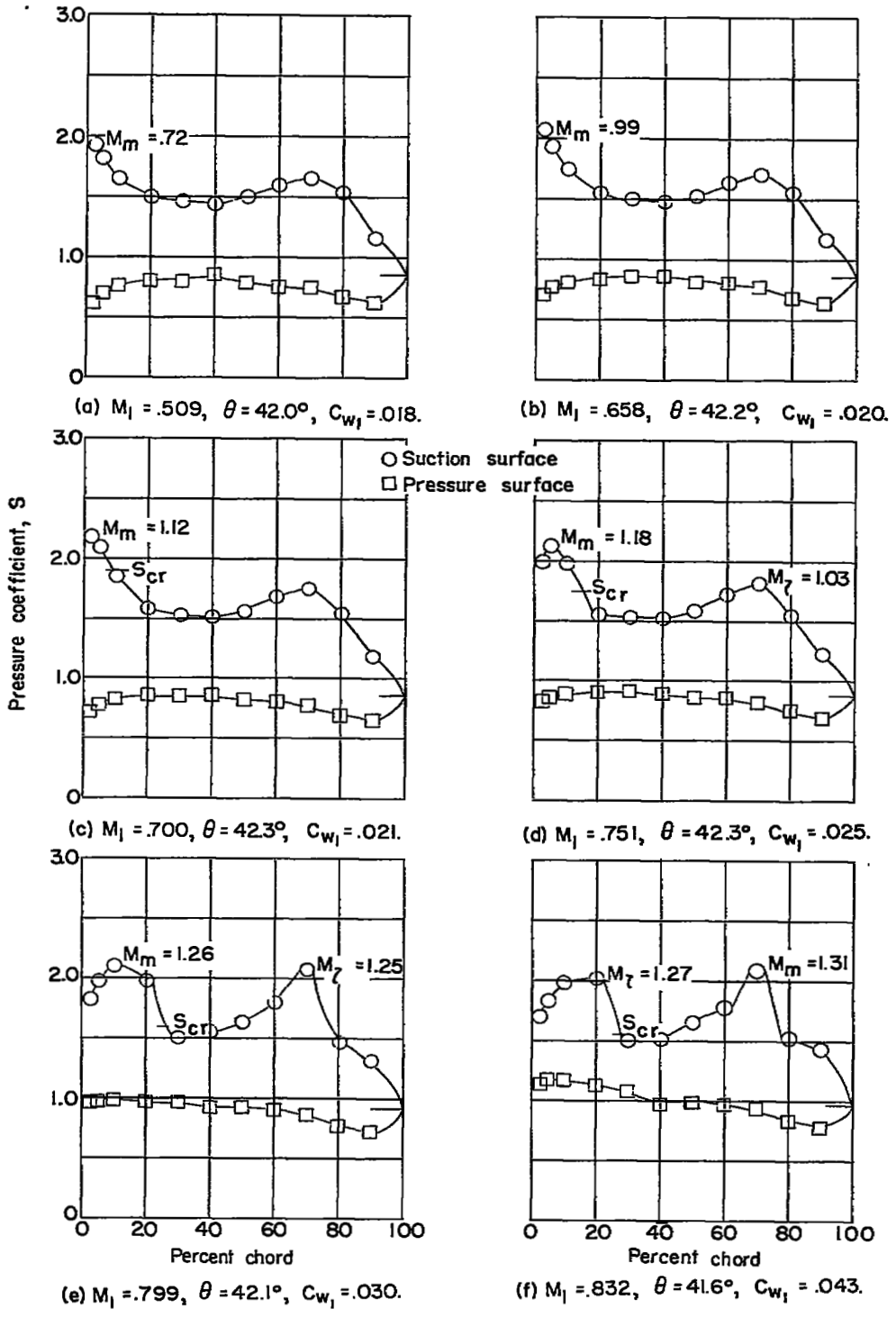

Figure 8.- Blade-surface pressure distribution and section characteristics for T1-$\left(18A_6I_{4b}\right)$08 blade at $\beta = 30.0°$, $\sigma = 1.5$, and $\alpha = 24.6°$.

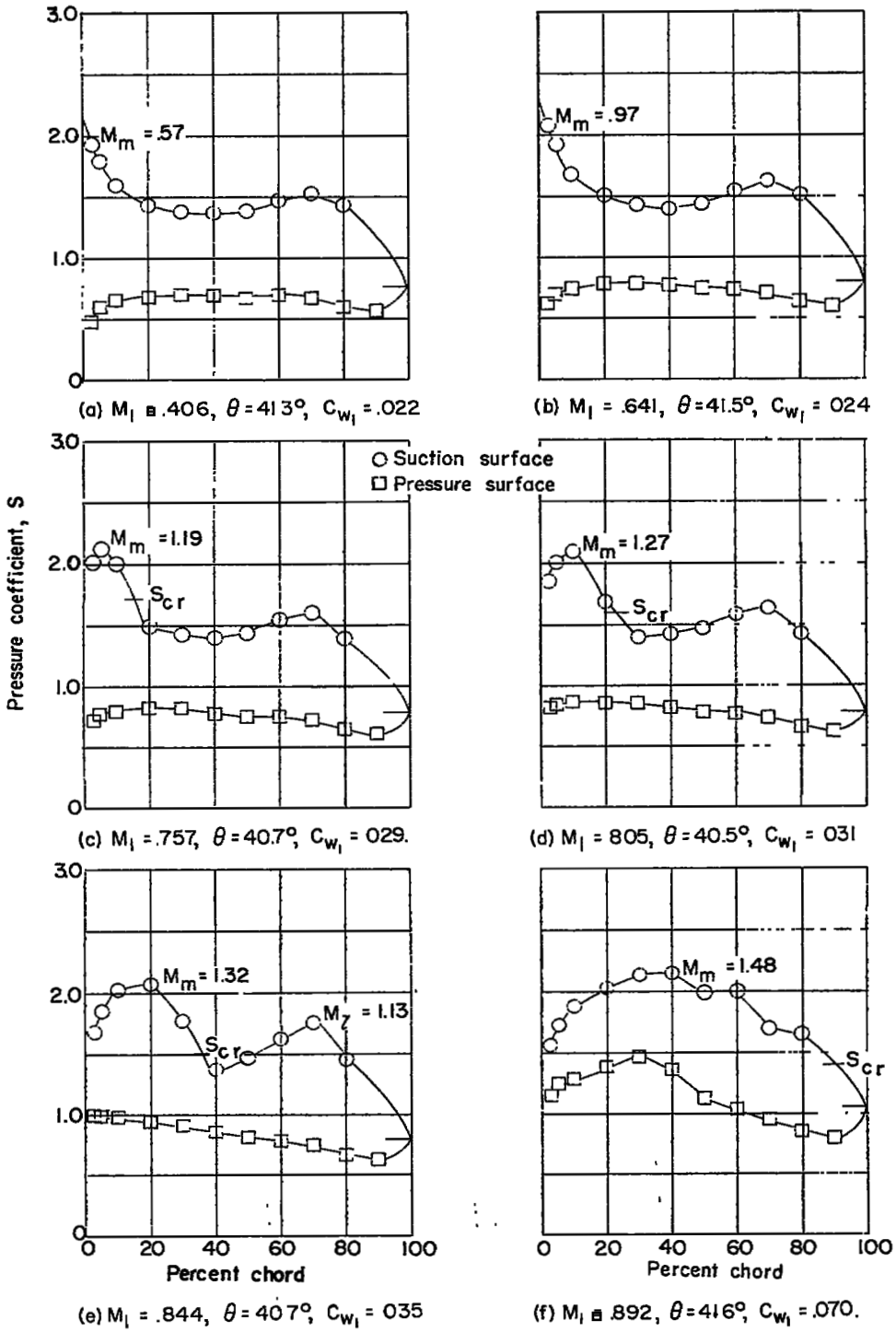

Figure 9.- Blade-surface pressure distribution and section characteristics for T1-$\left(18A_6I_{4b}\right)$08 blade at $\beta = 34.1^\circ$, $\sigma = 1.5$, and $\alpha = 25^\circ$.

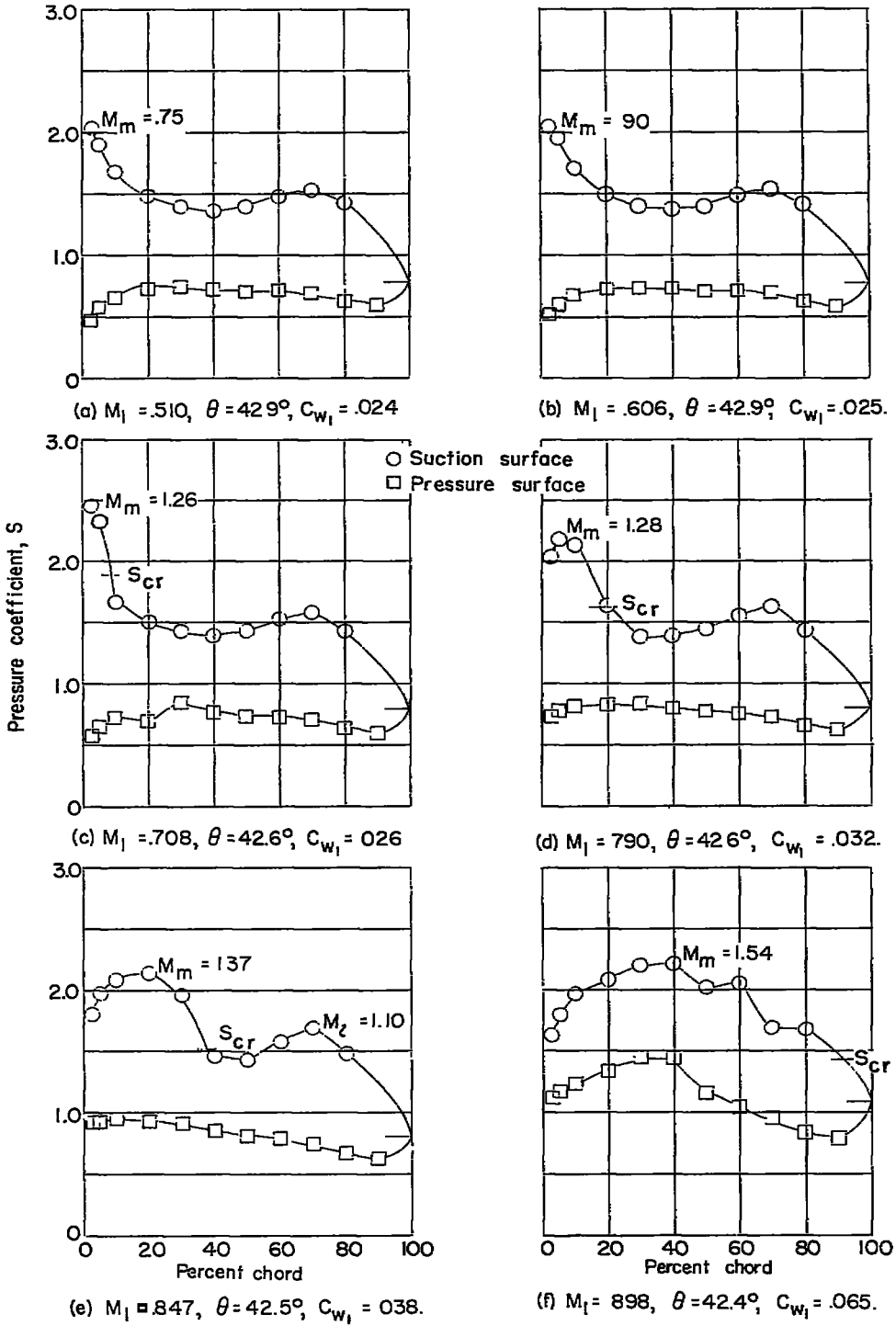

Figure 10.- Blade-surface pressure distribution and section characteristics for T1-$\left(18A_6I_{4b}\right)$08 blade at $\beta = 34.1°$, $\sigma = 1.5$, and $\alpha = 26.5°$.

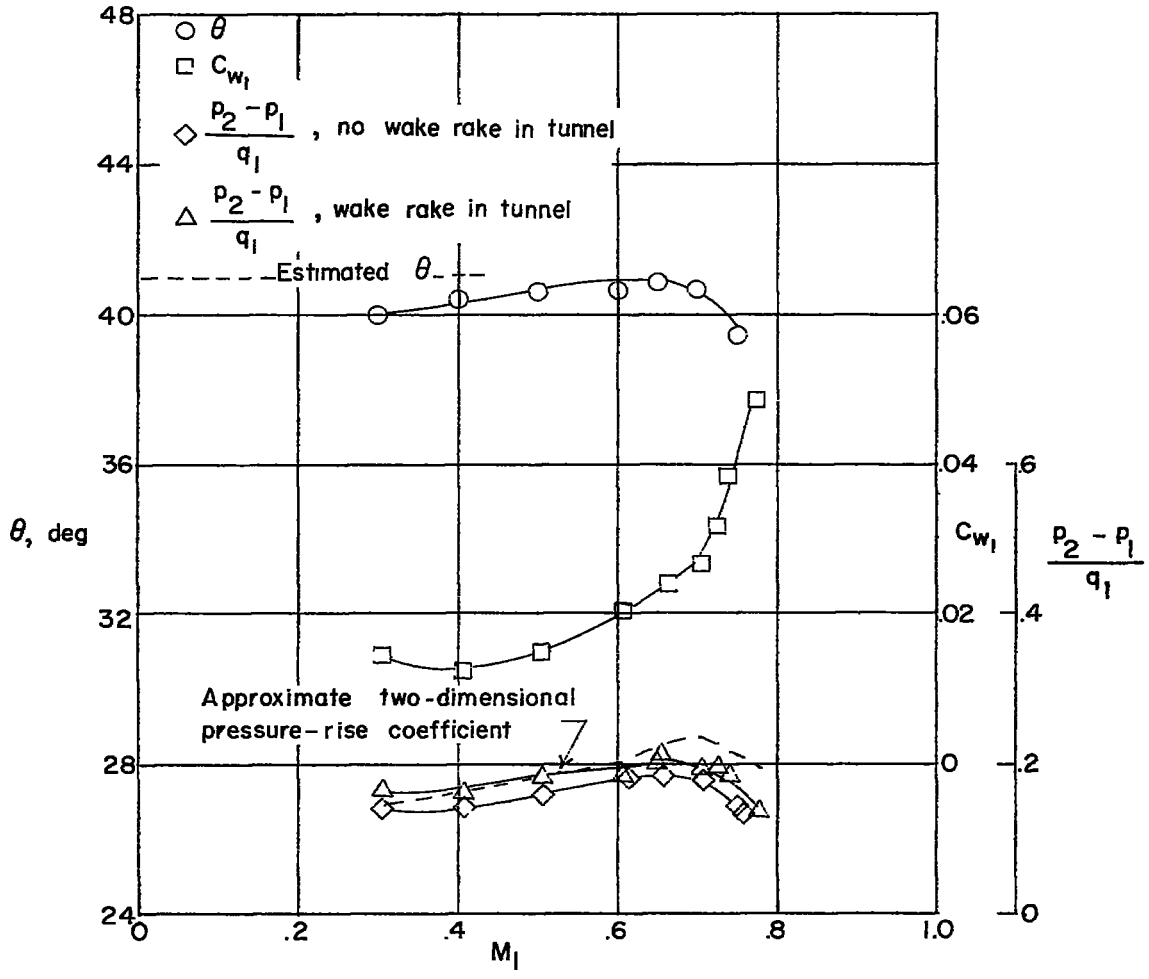

Figure 11.- Blade performance at $\beta = 26.9^\circ$, $\alpha = 21.5^\circ$, and $\sigma = 1.5$ for T1-$\left(18A_6I_{4b}\right)$08 blade section.

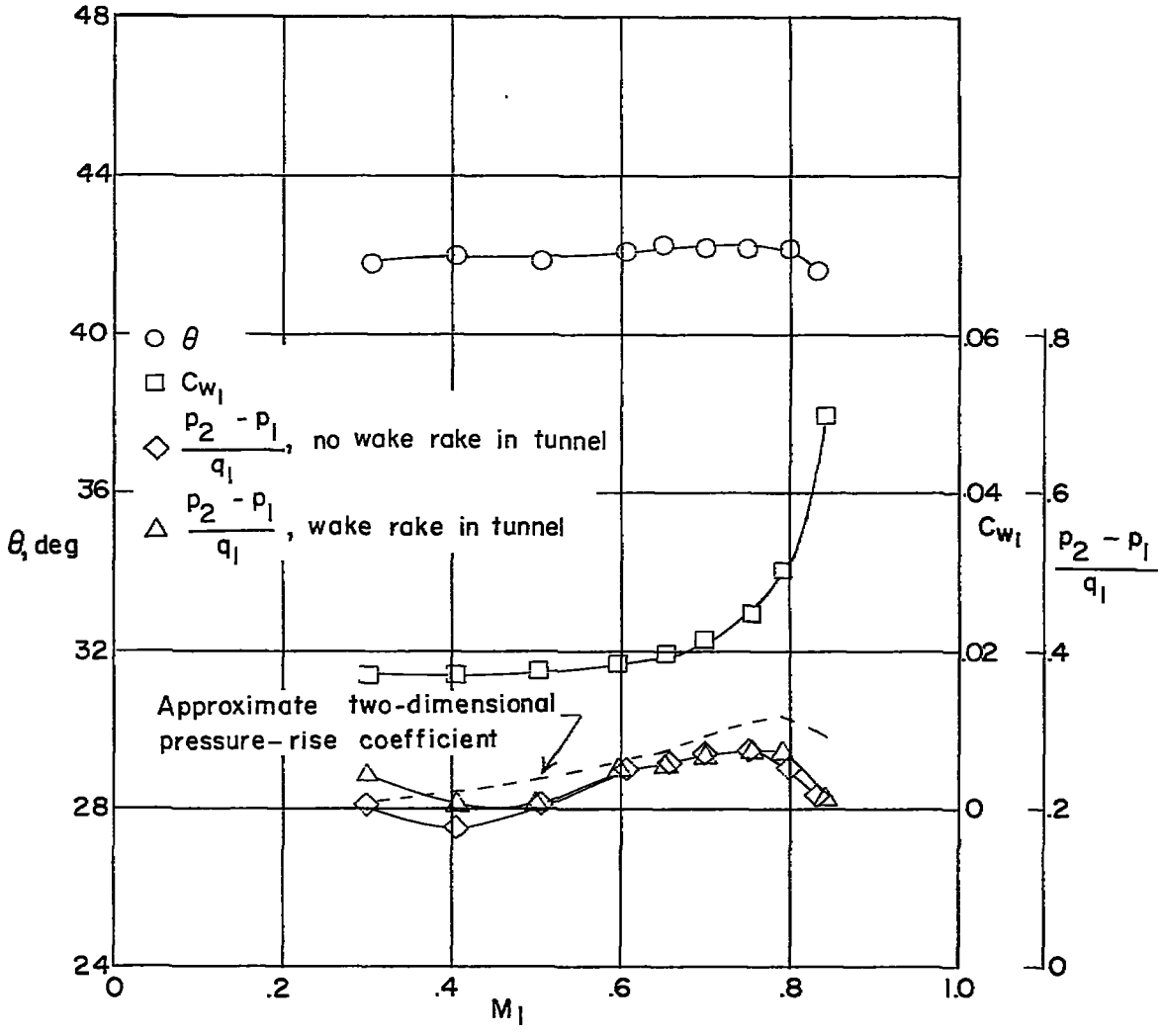

Figure 12.- Blade performance at $\beta = 30^\circ$, $\alpha = 24.6^\circ$, and $\sigma = 1.5$ for T1-$\left(18A_6I_{4b}\right)$08 blade section.

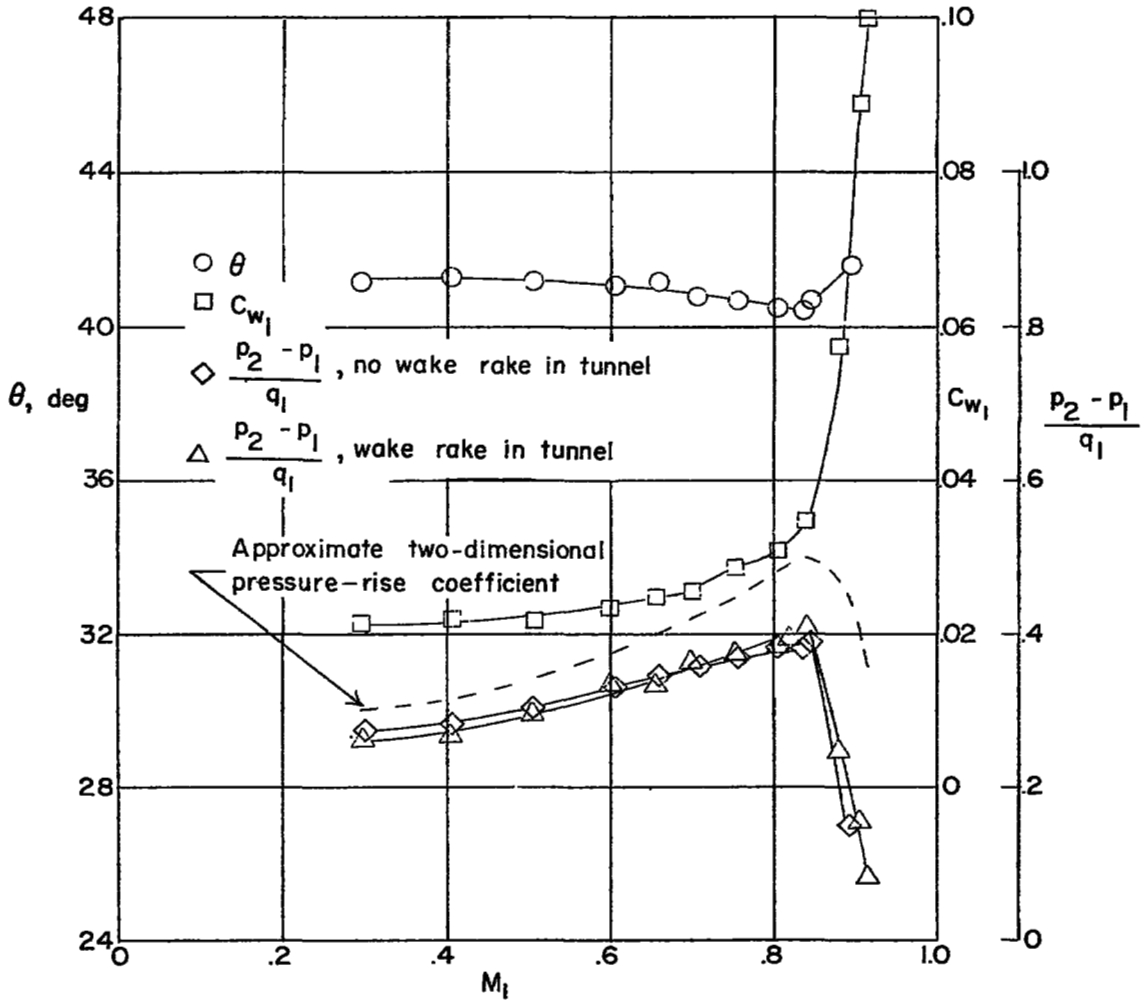

Figure 13.- Blade performance at $\beta = 34.1^\circ$, $\alpha = 25^\circ$, and $\sigma = 1.5$ for T1-$\left(18A_6I_{4b}\right)08$ blade section.

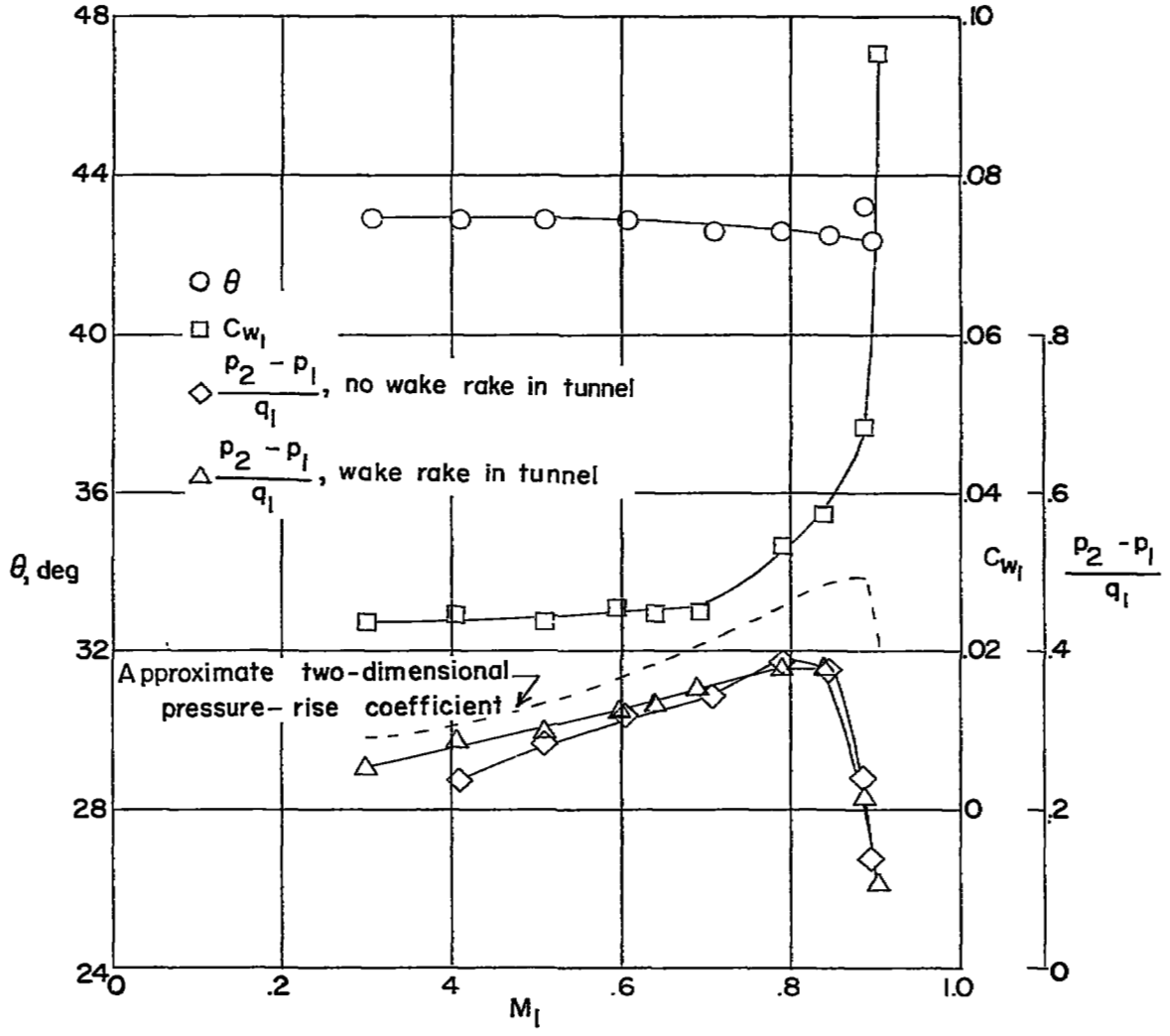

Figure 14.- Blade performance at $\beta = 34.1^\circ$, $\alpha = 26.5^\circ$, and $\sigma = 1.5$ for T1-$(18A_6I_{4b})$08 blade section.

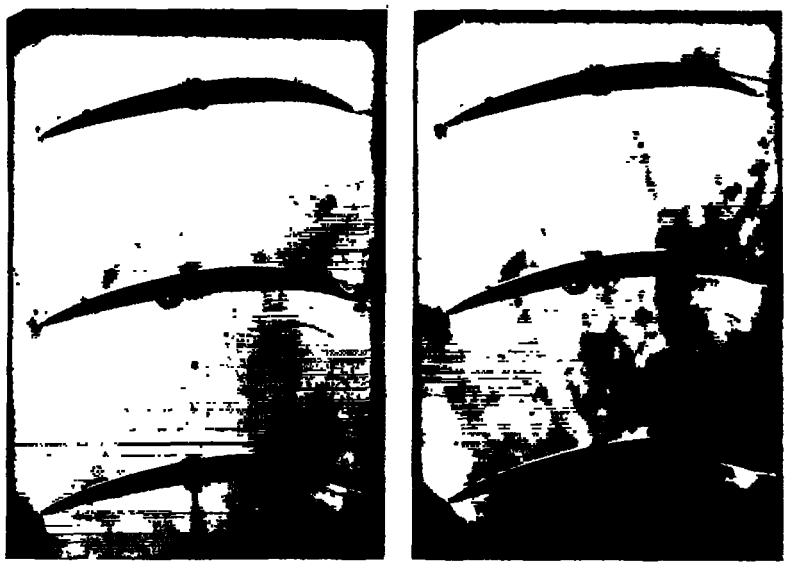

(a) $M_1 = 0.45$. (b) $M_1 = 0.60$.

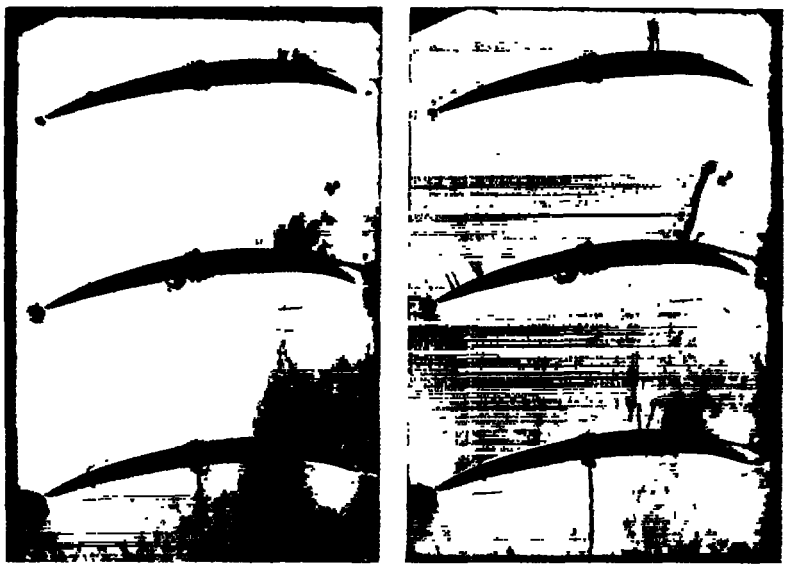

(c) $M_1 = 0.65$. (d) $M_1 = 0.70$.

L-89302

Figure 15.- Schlieren photographs for T1-$\left(18A_6I_{4b}\right)$08 blade at $\beta = 26.9°$, $\alpha = 21.5°$, and $\sigma = 1.5$.

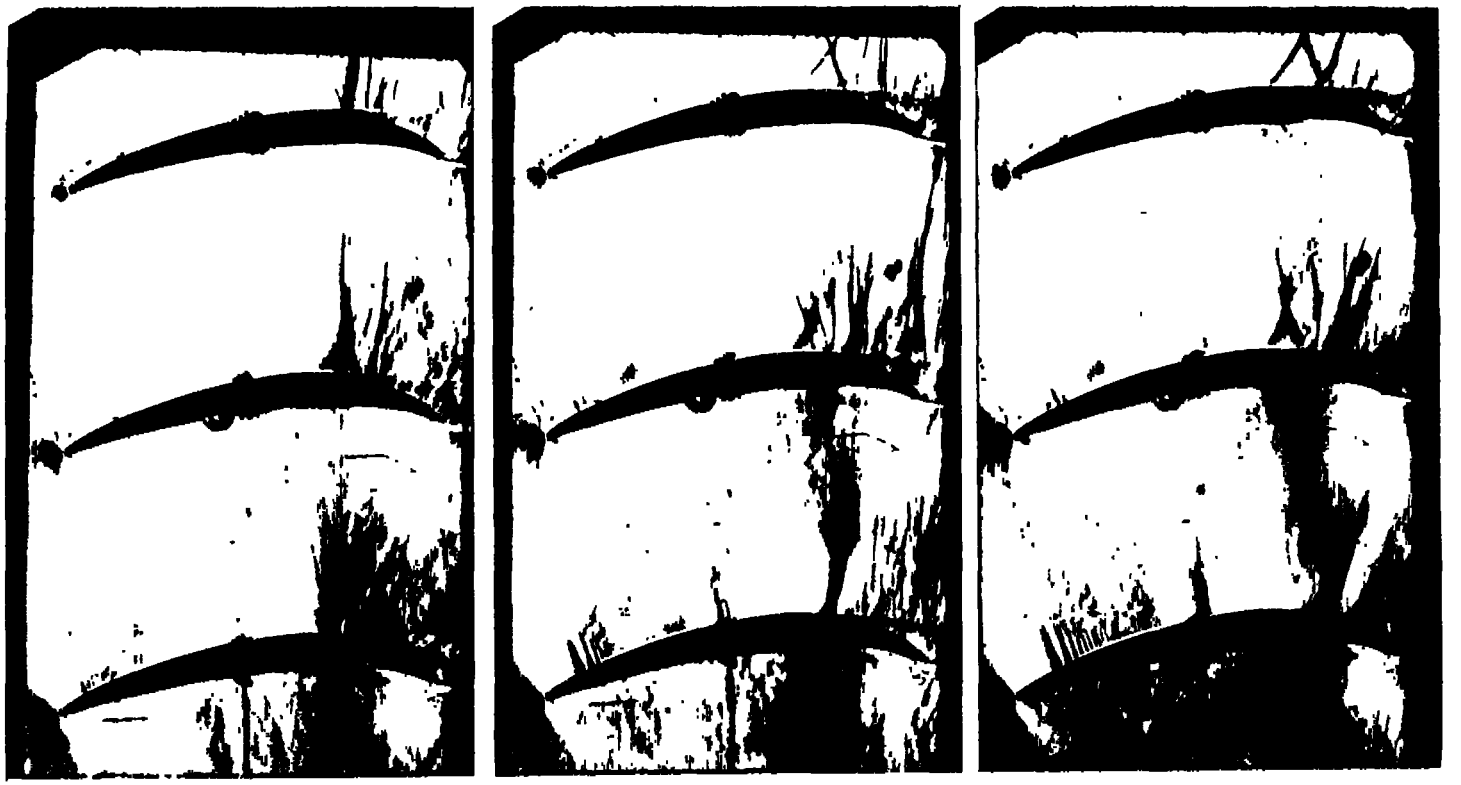

L-89303

(e) $M_1 = 0.74$. (f) $M_1 = 0.765$. (g) $M_1 = 0.78$.

Figure 15.- Concluded.

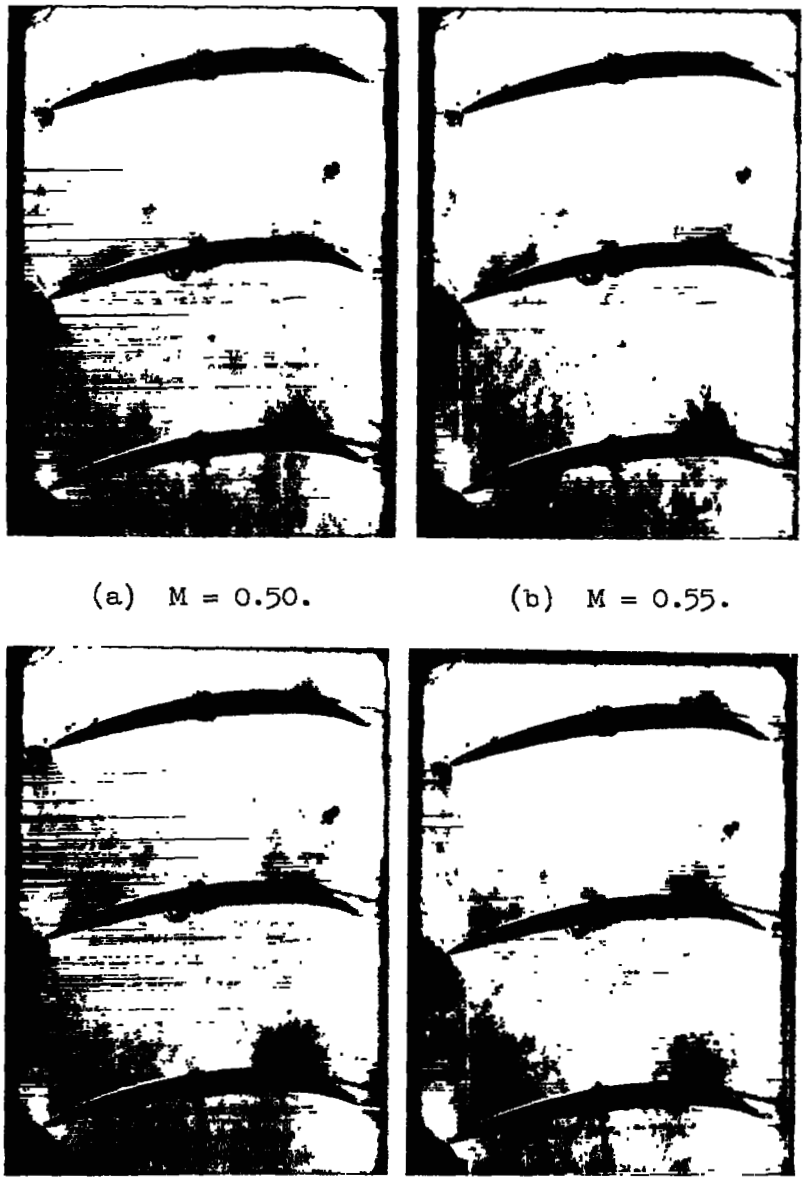

(a) M = 0.50. (b) M = 0.55.

(c) M = 0.60. (d) M = 0.65.

L-89304

Figure 16.- Schlieren photographs for T1-$(18A_6I_{4b})08$ blade at $\beta = 30.0^\circ$, $\alpha = 24.6^\circ$, and $\sigma = 1.5$.

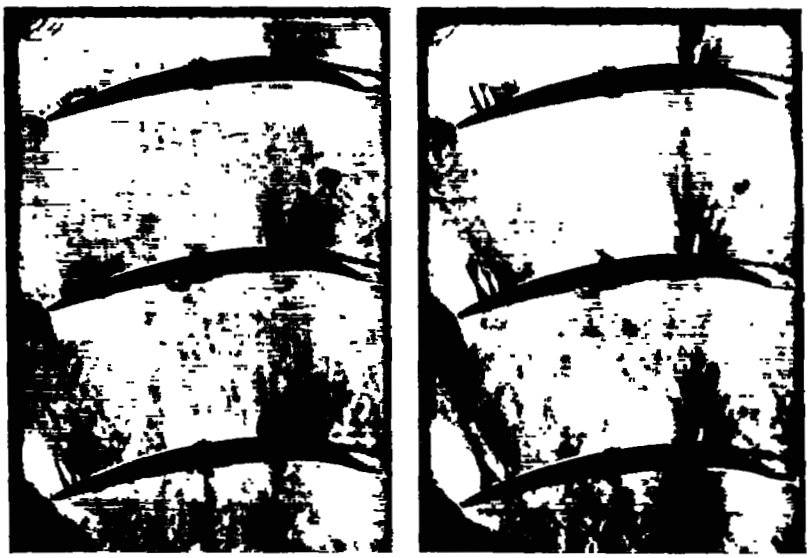

(e) M_1 = 0.70. (f) M_1 = 0.75.

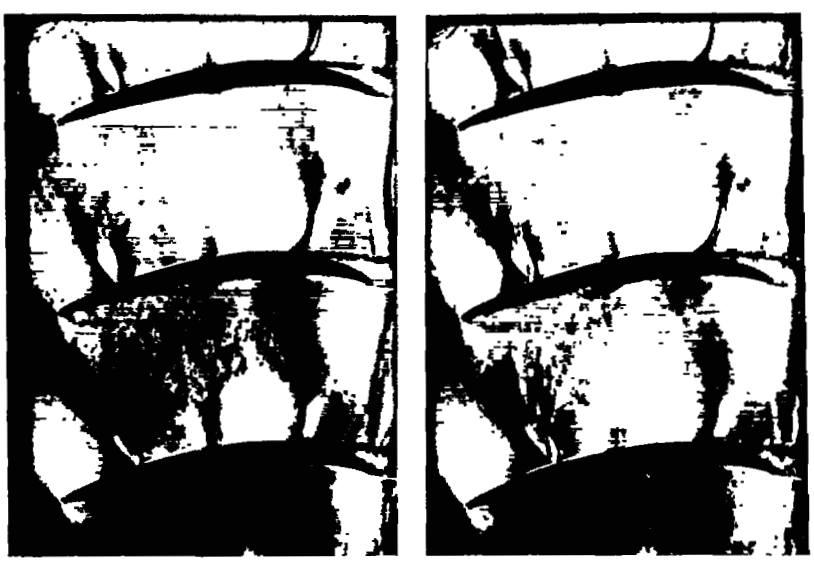

L-89305

(g) M_1 = 0.80. (h) M = 0.82.

Figure 16.- Concluded.

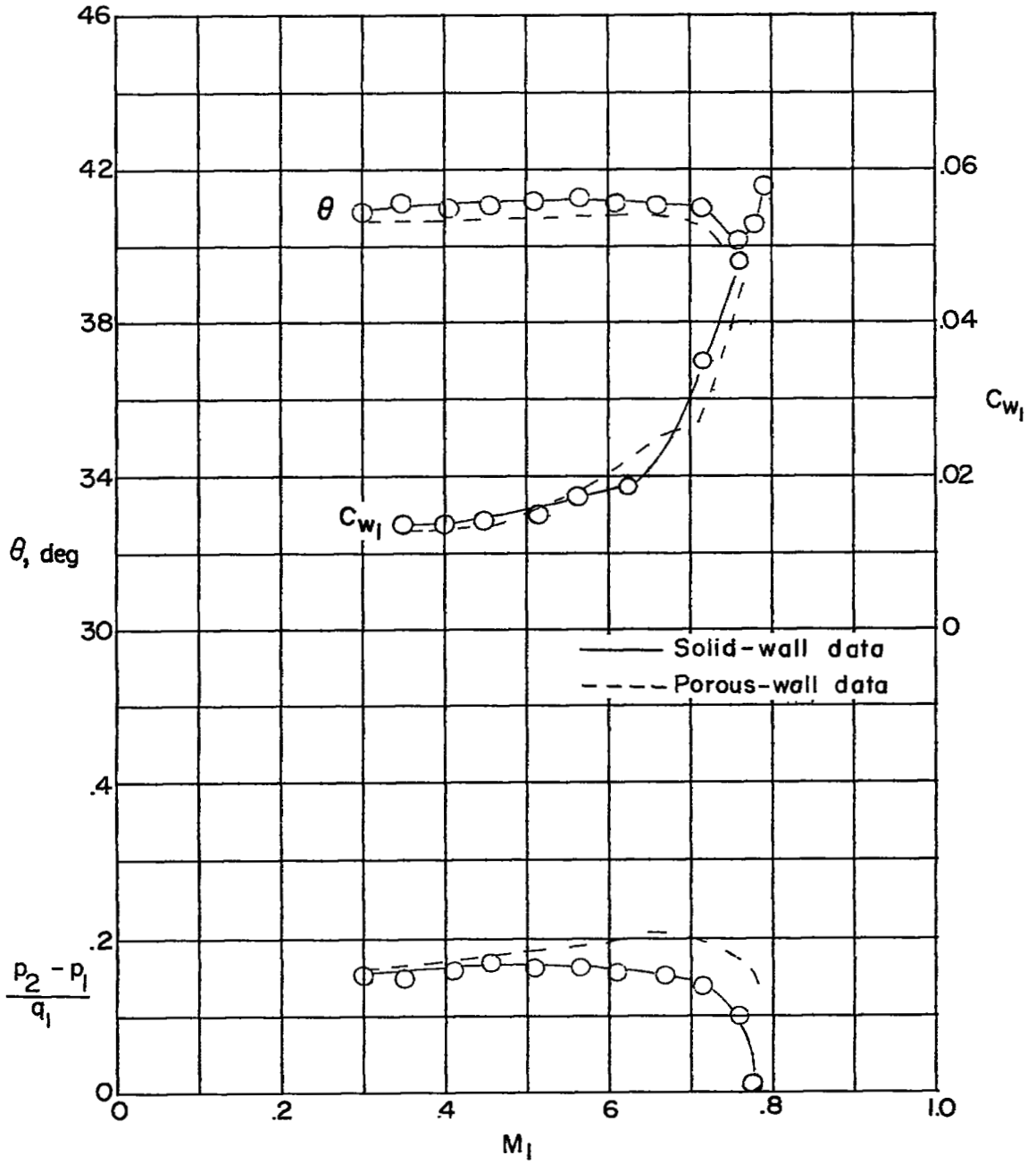

(a) $\beta = 26.9°$, $\alpha = 21.5°$, and $\sigma = 1.5$.

Figure 17.- Comparison of blade performance in cascade tunnels with both solid and porous side walls for T1-$\left(18A_6I_{4b}\right)$08 blade section.

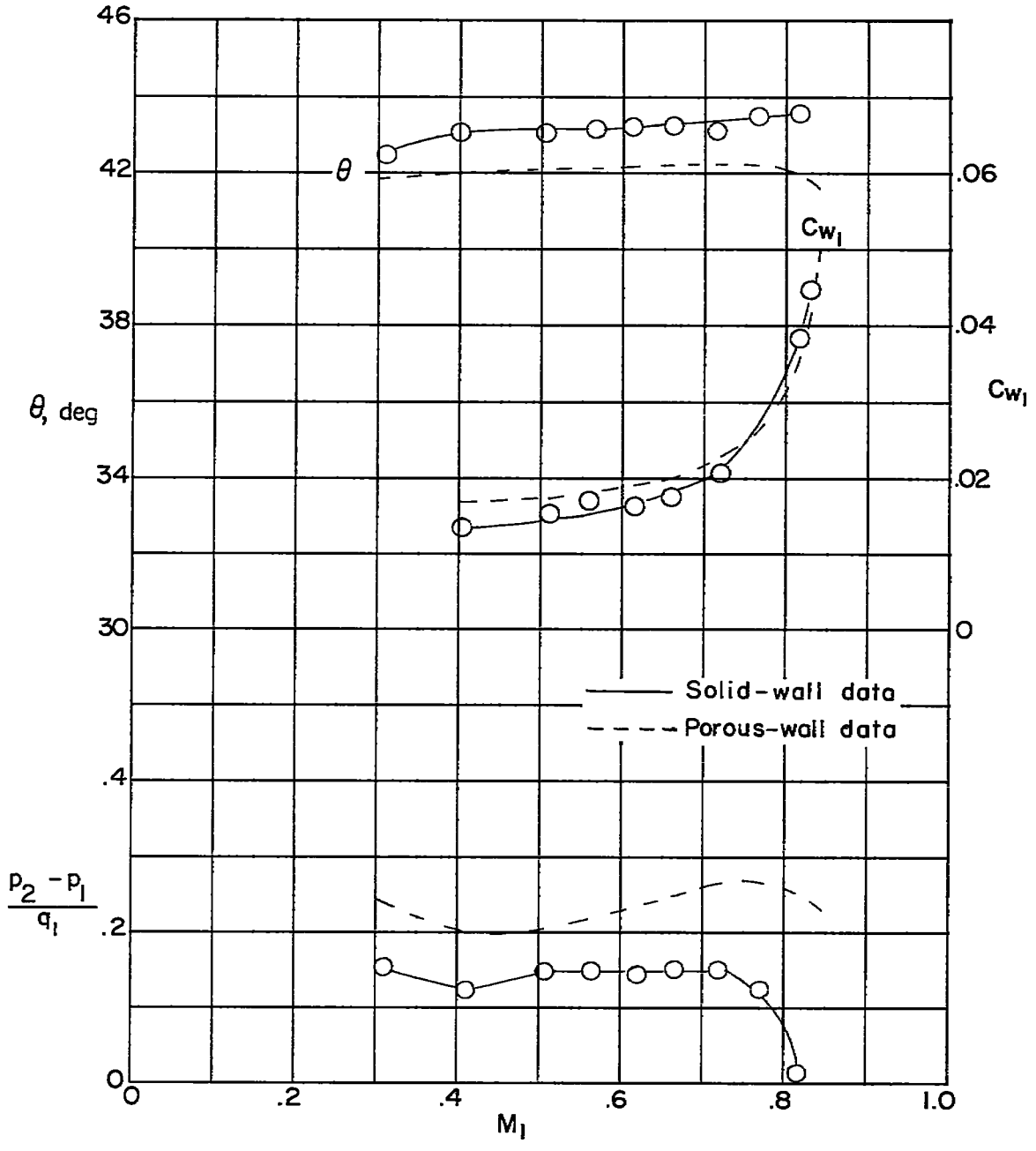

(b) $\beta = 30^\circ$, $\alpha = 24.6^\circ$, and $\sigma = 1.5$.

Figure 17.- Concluded.

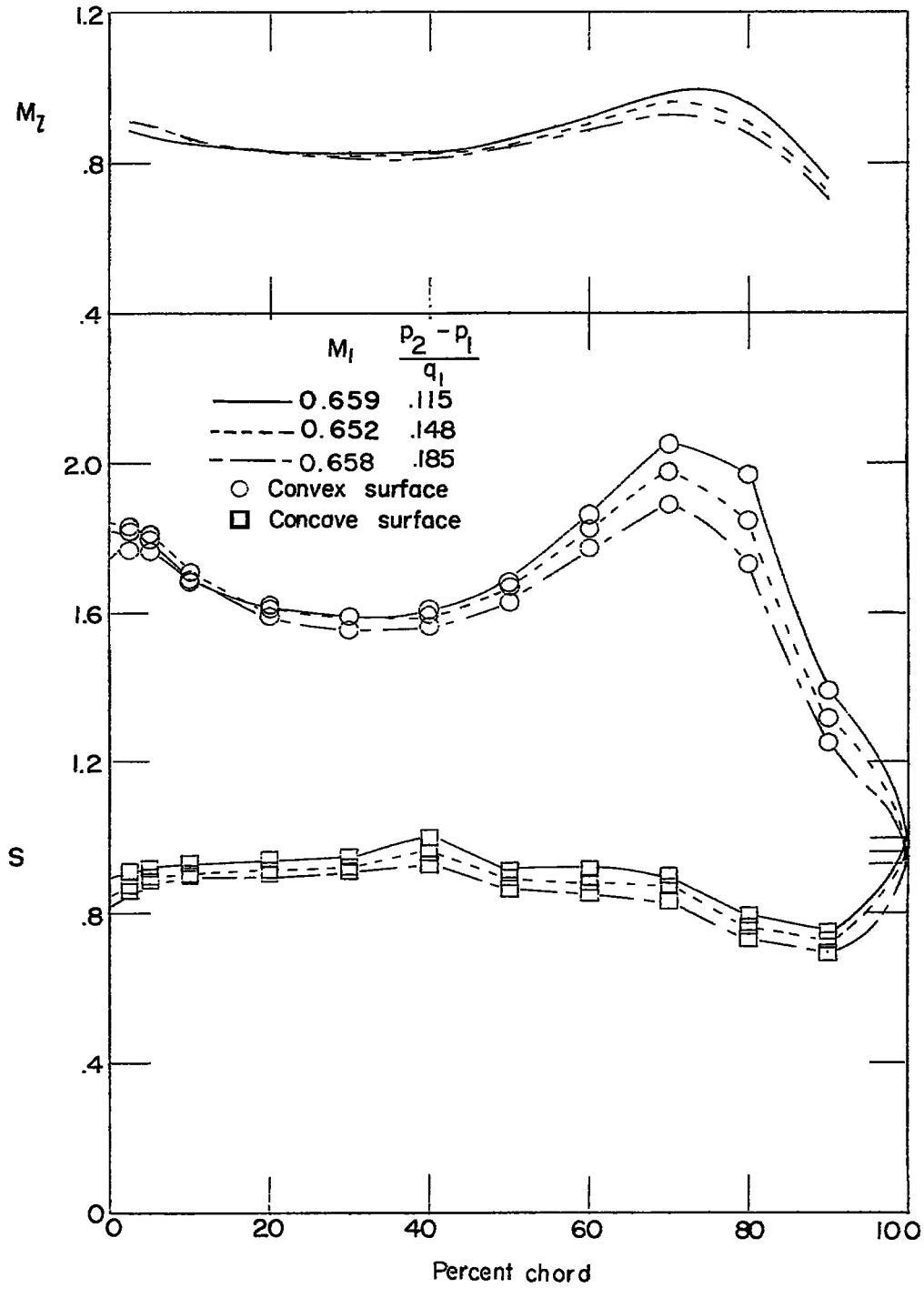

Figure 18.- Effect of pressure-rise coefficient on blade pressure distribution and local surface Mach number. $\beta = 26.9^\circ$, $\alpha = 21.5^\circ$, and $M_1 \approx 0.66$.

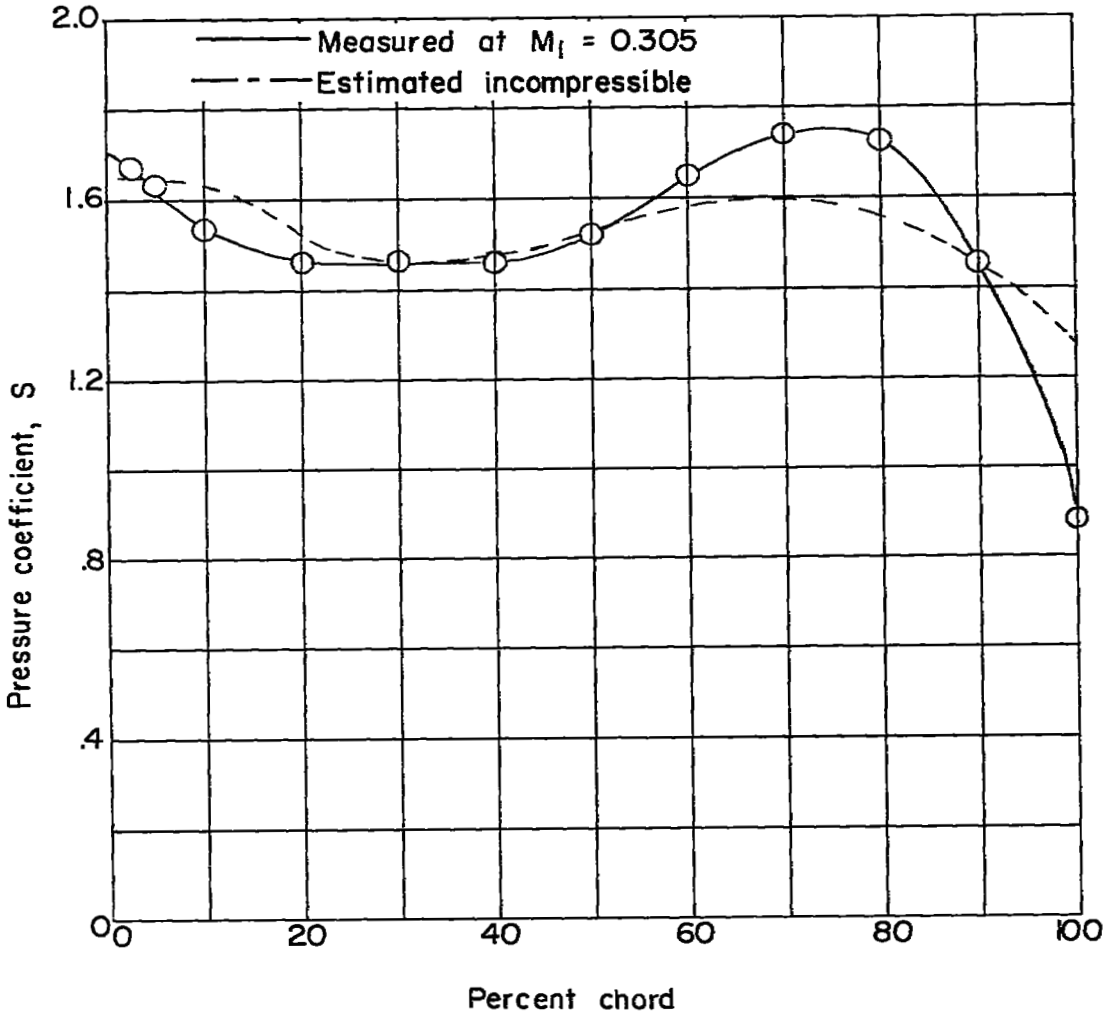

Figure 19.- Low-speed comparison between estimated and measured suction-surface pressure coefficients for T1-$(18A_6I_{4b})08$ blade at $\beta = 26.9^\circ$, $\alpha = 21.5^\circ$, and $\sigma = 1.5$.

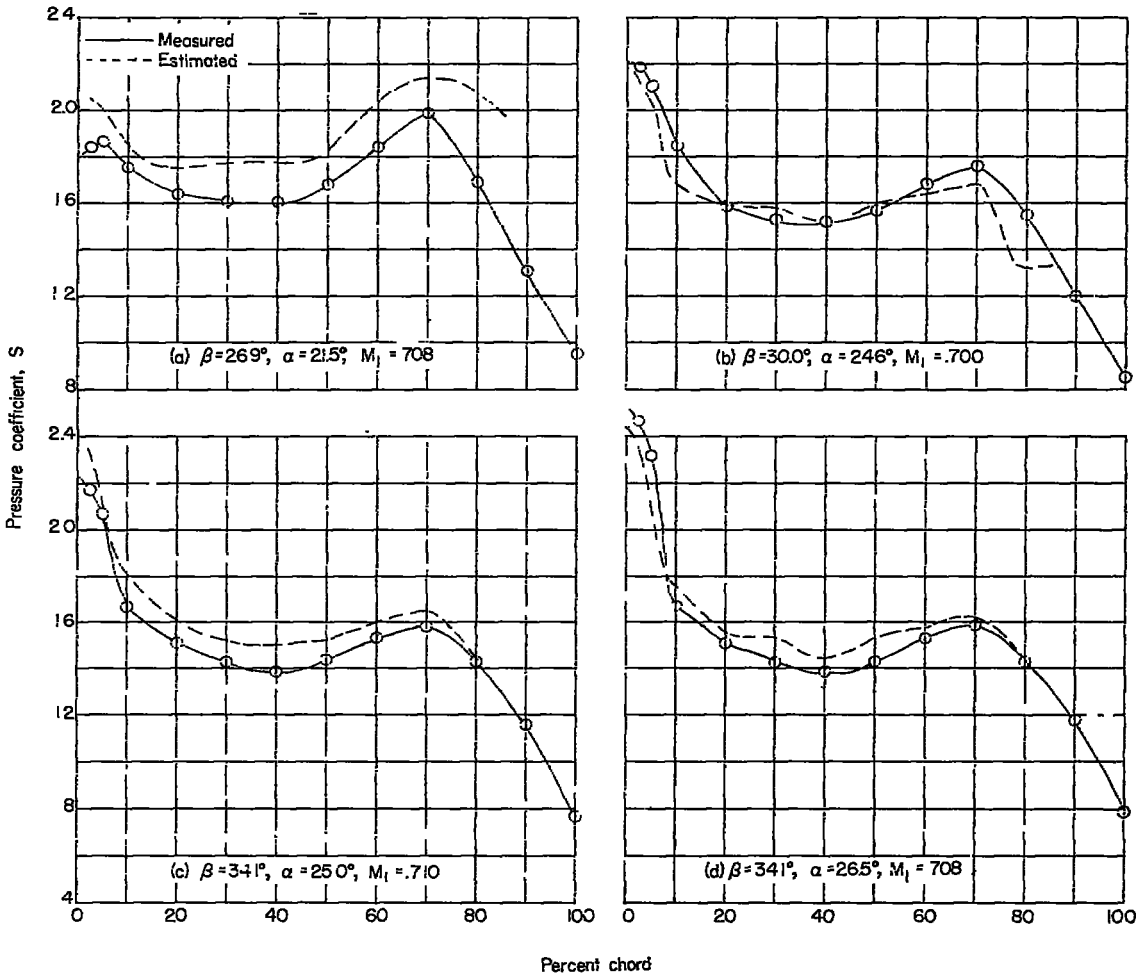

Figure 20.- Comparison between high-speed suction-surface pressure coefficients, measured at an inlet Mach number of approximately 0.7, and those obtained from an extrapolation of pressure coefficients, measured in low-speed tests at $M_1 = 0.30$, for all combinations of inlet angle and angle of attack tested for T1-$\left(18A_6I_{4b}\right)$08 blade at $\sigma = 1.5$.

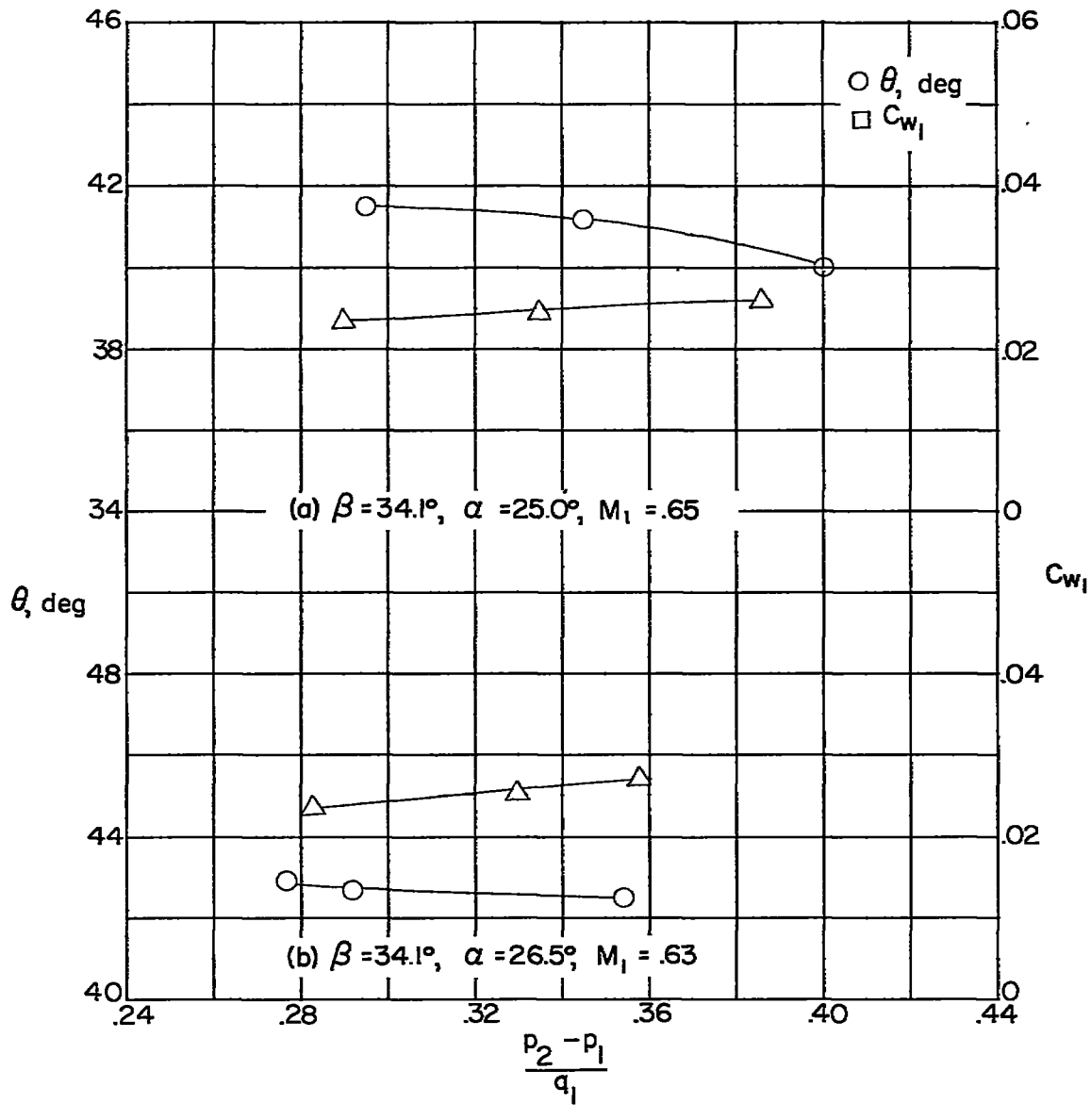

Figure 21.- Variation in turning angle and wake coefficient with change in back pressure induced by varying side-wall suction.

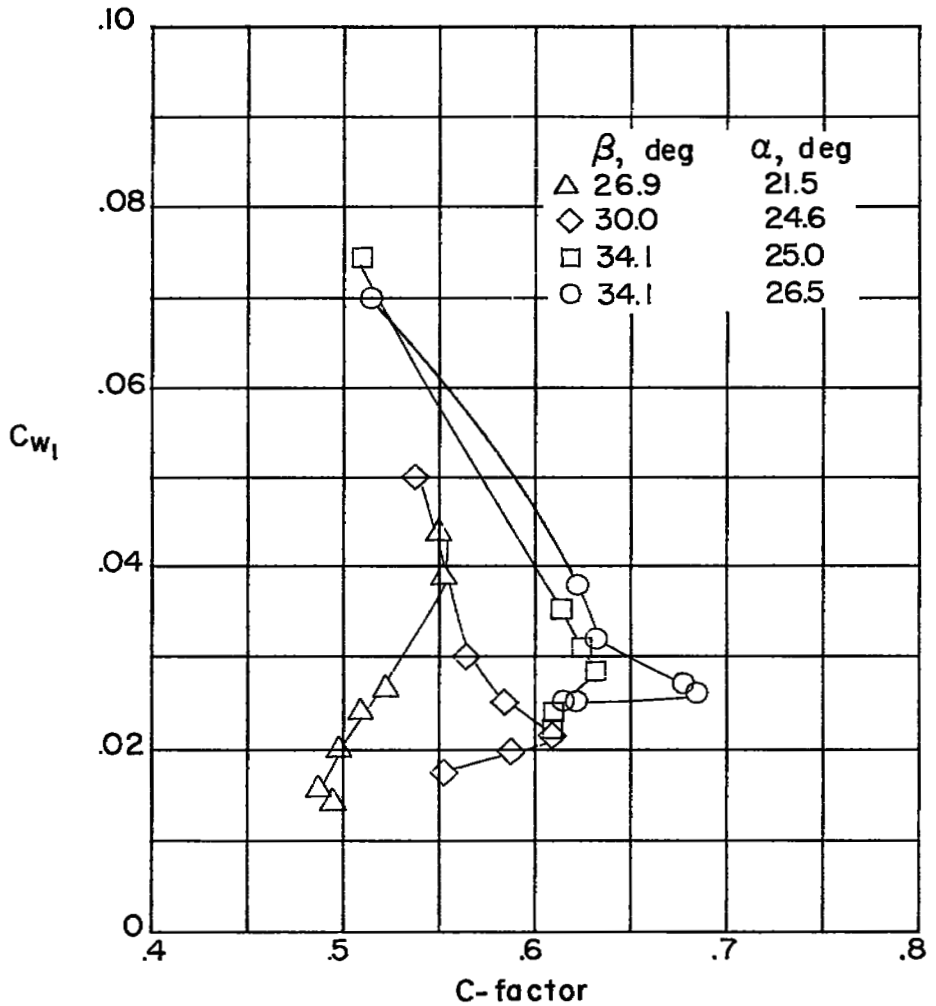

Figure 22.- Variation in momentum-loss coefficient with C-factor, where C-factor is equal to ratio of maximum static-pressure rise along blade surface to difference between stagnation and static pressures at peak surface-velocity point.

NACA - Langley Field, Va.

[redacted]